Supporting information

Dinuclear platinum(II) complexes emitting through TADF: new ligand design to minimise aggregation and the S_1–T_1 energy gap

Piotr Pander, Yana M. Dikova, Emma V. Puttock and J. A. Gareth Williams

Table of contents

1. General Experimental Details

Materials and methods for synthesis

Commercial chemicals were used as supplied without further purification. Reactions requiring an inert atmosphere were carried out using Schlenk-line techniques under an atmosphere of argon or nitrogen gas. Thin-layer chromatography analysis was performed on F_{254} silica plates and visualised by UV irradiation at 254 and 365 nm.

NMR spectra were recorded on a Bruker Avance-400 spectrometer (400 MHz), a Varian VNMRS-600 (600 MHz) or a Varian VNMRS-700 (700 MHz). Two-dimensional NMR experiments, including homonuclear correlation spectroscopy (COSY), heteronuclear multiple bond correlation spectroscopy (HMBC) and heteronuclear single quantum coherence spectroscopy (HSQC), were used to aid assignments. Chemical shift values (δ) are reported in parts per million (ppm) and coupling constants (J) in Hz. C^q denotes a quaternary carbon and the spectra are referenced to residual solvent peaks: $CDCl_3$ = 7.26 ppm (^{1}H), 77.16 ppm (^{13}C); DMSO = 2.50 ppm (^{1}H), 39.52 ppm (^{13}C). Multiplicity is as follows: s (singlet); d (doublet); t (triplet); q (quartet) and m (multiplet).

Electrospray ionisation mass spectra (ESI) were recorded using a Waters Acquity® TQD Tandem Quadrupole mass spectrometer with column using water containing formic acid (0.1% /v) and either acetonitrile or methanol as the carrier solvent. Atmospheric pressure solids analysis probe (ASAP) ionisation mass spectra were obtained using an LCT Premier XE mass spectrometer and an Acquity® UPLC from Waters Ltd at 350°C. High-resolution mass spectra were obtained using a Quantum time-of-flight (QTof) mass spectrometer.

Equipment and methods for photophysical measurements

All photoluminescence measurements were conducted in solutions degassed with three freeze-pump cycles, unless otherwise stated. Thin films in polystyrene were deposited from chloroform solutions. The films were fabricated by spin-coating and dried under vacuum at room temperature. Absorption spectra in solution were recorded with a UV-3600 (Shimadzu) or Biotek Instruments XS double beam spectrophotometer. Photoluminescence (PL) spectra in solutions were recorded using a QePro compact spectrometer (Ocean Optics). Time-resolved decays in solution were recorded with a Horiba DeltaFlex TCSPC system using a 405 nm

DeltaDiode or 330 nm SpectraLED light sources. Photoluminescence decays in film were recorded using nanosecond gated luminescence and lifetime measurements (from 400 ps to 1 s) using the third harmonic (355 nm) of a high-energy pulsed Nd:YAG laser (EKSPLA). The emitted light was focused onto a spectrograph and detected with a sensitive gated iCCD camera (Stanford Computer Optics) having sub-nanosecond resolution. Time-resolved measurements were performed by exponentially increasing gate and integration times. Further details are available in an earlier work.[1] Temperature-dependent experiments were conducted using a liquid nitrogen cryostat VNF-100 (sample in flowing vapour, Janis Research) under nitrogen atmosphere. Emission spectra in solid state were obtained using an integrating sphere (Labsphere) coupled with a 365 nm LED light source and QePro (Ocean Optics) detector.

Determination of photoluminescence quantum yields in solution

Photoluminescence quantum yields were obtained from the gradient of a plot of the total photoluminescence intensity versus absorbance at λ_{ex} (same for both standard and analyte), obtained over a range of concentrations for both the analyte and standard, equation S1. Concentrations in the range 10^{-6} – 10^{-5} M were used, over which there is a linear correlation between PL intensity and absorbance, while the absorbance of the standard was maintained < 0.05. The standard was rhodamine 6G in air-equilibrated absolute ethanol solution, Φ = 0.91. [2]

$$\Phi_x = \Phi_{standard}\left(\frac{grad_x}{grad_{standard}}\right)\left(\frac{\eta_x^2}{\eta_{standard}^2}\right) \qquad \textbf{Equation S1}$$

Here, Φ_x, $\Phi_{standard}$ are the photoluminescence quantum yield of the analyte and standard, respectively; $grad_x$, $grad_{standard}$ are the gradients of the best linear fits of PL intensity versus absorbance at λ_{ex} for the analyte and standard, respectively; η_x and $\eta_{standard}$ are the refractive indices of the solvents used for the analyte and standard, respectively.

Procedure for fitting PL decay time versus temperature

The dependence of the observed lifetime with temperature is well fitted using the model described by Equation S2,[3,4] where $\tau_{obs}(T)$ is the observed emission lifetime (s); ΔE_{ST} is the S_1-T_1 energy splitting J mol^{-1}; τ_{PH} is the phosphorescence lifetime (s); k_r^S is the radiative rate constant of the singlet state (s^{-1}); R is the universal gas constant, 8.314 J mol^{-1} K^{-1}; and T is the temperature in K.

$$\tau_{obs}(T) = \frac{3 + e^{-\frac{\Delta E_{ST}}{RT}}}{\frac{3}{\tau_{PH}} + k_r^S e^{-\frac{\Delta E_{ST}}{RT}}}$$ **Equation S2**

OLED devices

OLEDs were fabricated by spin-coating / evaporation hybrid method. The hole injection layer (PEDOT AI4083), hole transport layer PVKH, and emitting layer (TCTA:PO-T2T + dopant, mCP:PO-T2T + dopant, mCP:PBD + dopant) were spin-coated, whereas the electron transport layer (PO-T2T or TmPyPB) and cathode (LiF/Al) were evaporated. The devices were of 4×2 mm pixel size. 2,4,6-Tris[3-(diphenylphosphinyl)phenyl]-1,3,5-triazine (PO-T2T, LUMTEC), tris(4-carbazoyl-9-ylphenyl)amine (TCTA, LUMTEC), 1,3-bis(carbazol-9-yl)benzene (mCP, sublimed, LUMTEC), 2-(4-biphenyl)-5-(4-*tert*-butylphenyl)-1,3,4-oxadiazole (PBD, Sigma Aldrich), poly(*N*-vinylcarbazole) (PVKH, Sigma Aldrich, M = 10^6 Da), 1,3,5-tri[(3-pyridyl)-phen-3-yl]benzene (TmPyPB, Lumtec), LiF (99.995%, Sigma Aldrich), and aluminium pellets (99.9995%, Lesker) were purchased from the companies indicated in the parentheses. Pre-patterned indium-tin-oxide (ITO) on glass substrate was used, with a sheet resistance of 20 Ω/sq and ITO thickness of 100 nm. The substrates were cleaned by sonicating in acetone and subsequently in isopropanol for 15 minutes each and then treated with oxygen plasma for 6 minutes at full power. PEDOT AI4083 was spun-coated and annealed on a hotplate at 120 ˚C for 15 min to give a 30 nm film. The emitting layer was deposited either from a chloroform : chlorobenzene (95:5 v/v) solution (20 mg mL^{-1} total solids content), for the TCTA:PO-T2T host, or from a toluene solution (10 mg mL^{-1} total solids content) for mCP:PO-T2T and mCP:PBD hosts. The dopant was dissolved in the solution of blend host in order to obtain the final 3% or 5% concentration in the emitting layer. All solutions were filtered directly before use with a PVDF (organic solvents) and PES (PEDOT AI4083) syringe filter with 0.45 μm pore size. All other layers were thermally evaporated using Kurt J. Lesker Spectros II deposition system at 10^{-6} mbar base pressure. All organic materials and aluminium were deposited at a rate of 1 Å s^{-1}. The LiF layer was deposited at a rate of 0.1–0.2 Å s^{-1}. Characterisation of OLED devices was conducted in a 10 inch integrating sphere (Labsphere) connected to a Keithley 2400 Source Measure Unit and coupled with a QePRO (Ocean Optics) spectrometer. Further details are available in earlier work.[5]

Calculations

We use density functional theory (DFT) and time-dependent DFT (TD-DFT) as well as the quasi-degenerate perturbation theory (QDPT)[6,7] with zeroth-order regular approximation (ZORA)[8,9] implemented in Orca 5.0.3[10,11] in order to gain additional insights into the luminescence mechanisms in **5** and **6**. Ground state (S_0) and triplet excited state (T_1) geometries were optimised at the B3LYP/def2-SVP[12] level of theory which was found to be the most optimal for this task. We used def2/J[13] auxiliary basis set and atom-pairwise dispersion correction with the Becke-Johnson damping scheme (D3BJ).[14,15] All geometries were verified to be true energy minima by a frequency calculation. All optimisations were performed with tight SCF and geometry convergence criteria. Excited state energy of TD-DFT states was calculated using the resultant S_0 or T_1 geometry at the B3LYP/def2-TZVP[12] level of theory. In this case, relativistically-corrected triple-zeta basis sets with the zeroth-order regular approximation (ZORA)[8,9] were used: ZORA-def2-TZVP[12] with the SARC/J[16] auxiliary basis for all atoms except Pt and I, for which a segmented all-electron relativistically-contracted (SARC) SARC-ZORA-TZVP[16] basis set was used. Spin-orbit coupling (SOC) calculations were performed as implemented in the ORCA software. SOC matrix elements (SOCME) and SOC-corrected excitations (SOC states) were computed using the same settings. The RI-SOMF(1X) setting was used to accelerate SOC calculations. All molecular orbital (MO) iso surfaces were visualised using Gabedit 2.5.0.[17]

2. Synthetic details and characterisation of compounds **1** – **7**

Compound 1

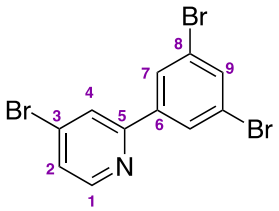

3,5-Dibromophenylboronic acid (1.68 g, 6.00 mmol), 2,4-dibromopyridine (1.50 g, 6.33 mmol), Na_2CO_3 (6.36 g, 60.00 mmol), and tetrakis(triphenylphosphine)palladium(0) (0.52 g, 0.45 mmol) were added to a round-bottom flask. Water (30 mL), ethanol (30 mL), and toluene (60 mL) were added. The flask was immediately evacuated and backfilled with nitrogen five times after which it was heated under a nitrogen atmosphere to 70 °C for 2 h and then to 90 °C for 18 h. The mixture was then cooled to RT, diluted with 100 mL of deionised water and extracted with CH_2Cl_2 (4 × 100 mL). The extracts were collected, dried with anhydrous $MgSO_4$, filtered, and the solvent evaporated. The product was obtained purified by gradient flash column chromatography with petroleum ether:CH_2Cl_2 mixture as the mobile phase (90:10→80:20). A batch of 0.69 g of product was obtained as white crystals by evaporating down the main fraction, while an additional 0.13 g was obtained by crystallisation from the remaining fractions; total yield 0.82 g, 35%.

^{1}H NMR (599 MHz, $CDCl_3$) δH / ppm 8.51 (1H, dd, J 5.5, 0.5, H^1), 8.07 (2H, d, J = 2.0, H^7), 7.86 (1H, dd, J = 2.0, 0.5, H^4), 7.73 (1H, t, J = 2, H^9), 7.46 (1H, dd, J = 5.5, 2.0, H^2). ^{13}C NMR (151 MHz, $CDCl_3$) δC / ppm 155.7 C^5, 150.5 C^1, 141.3 C^6, 134.9 C^9, 133.8 C^3, 128.8 C^7, 126.4 C^2, 124.0 C^4, 123.5 C^8. HRMS (ESI^+) *m/z* 389.8147 $[M+H]^+$, calc. 389.8129 for $[C_{11}H_7Br_3N]$.

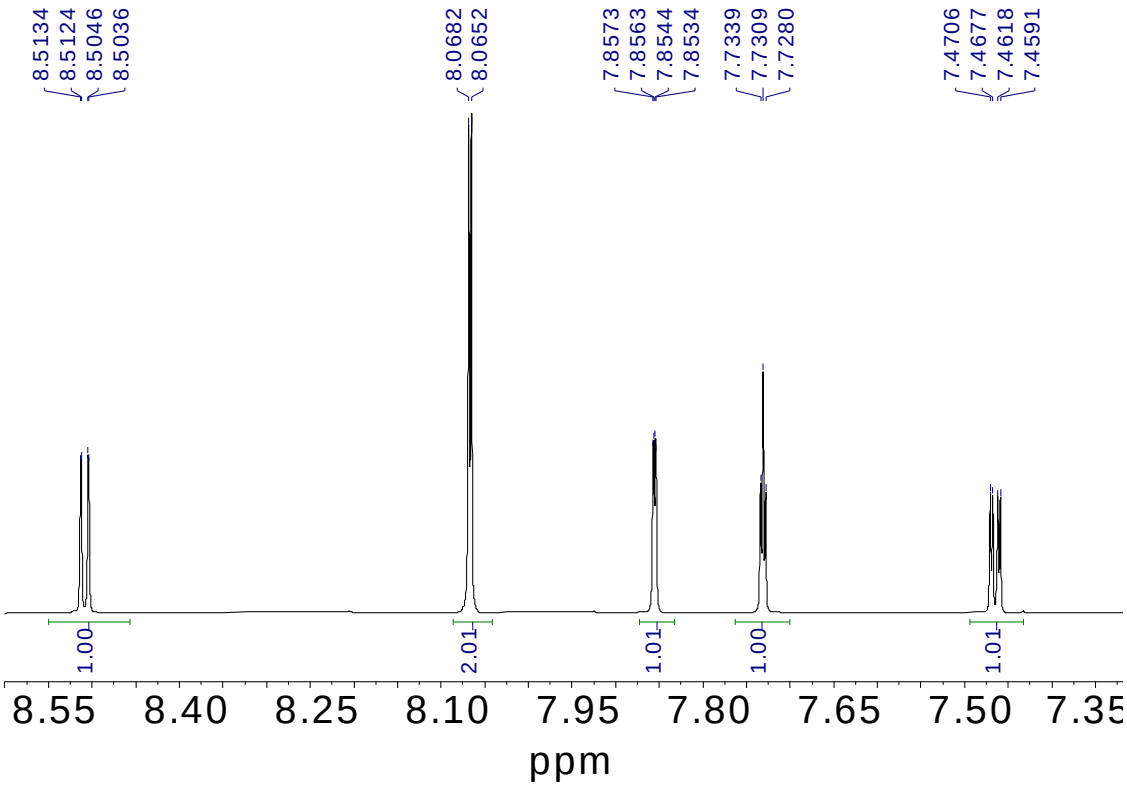

Figure S2.1. ^{1}H NMR spectrum of **1** in $CDCl_3$ at 599 MHz.

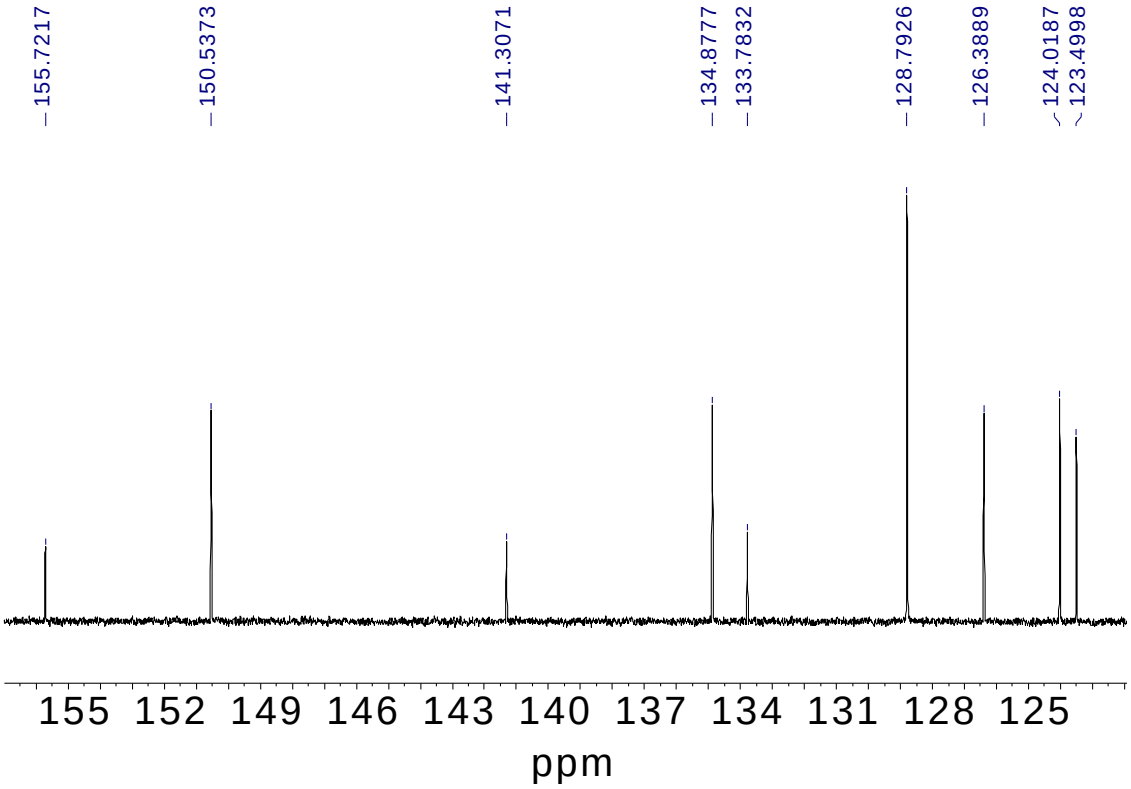

Figure S2.2. ^{13}C NMR spectrum of **1** in $CDCl_3$ at 151 MHz.

Compound 2

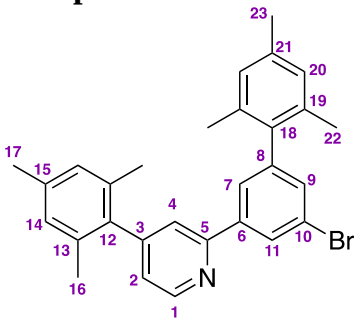

Compound **1** (0.300 g, 0.77 mmol), 2,4,6-trimethylphenylboronic acid (0.330 g, 2.01 mmol), $Pd(PPh_3)_4$ (0.142 g, 0.12 mmol), Cs_2CO_3 (5.00 g, 15.4 mmol) and anhydrous toluene (18 mL) were added to a Schlenk flask. The mixture was immediately evacuated and backfilled with nitrogen five times and then heated to 90°C for 18h. The mixture was then cooled to RT, diluted with 50 mL of deionised water and extracted with CH_2Cl_2 (3 × 40 mL). The extracts were collected, dried with anhydrous $MgSO_4$, filtered and evaporated down. The final product was obtained by purification using gradient flash column chromatography with a column loaded with 24 g of silica and using petroleum ether:ethyl acetate mixture as the mobile phase (100:0→100:1). The product was obtained as an off-white powder (0.24 g, 67%).

^{1}H NMR (400 MHz, $CDCl_3$) δH / ppm 8.65 (1 H, dd, J 5.0, 0.9, H^1), 8.11 (1 H, dd, J 1.7, H^{11}), 7.63 (1 H, dd, J 1.6, H^7), 7.43 (1 H, m, H^4), 7.27 (1 H, dd, J 1.6, H^9), 7.00 (1 H, dd, J 5.0, 1.5, H^2), 6.89 (2 H, s, H^{14}), 6.85 (2 H, s, H^{20}), 2.25 (3 H, s, H^{17}), 2.23 (3 H, s, H^{23}), 1.96 (6 H, s, H^{22}), 1.94 (6 H, s, H^{16}). ^{13}C NMR (101 MHz, $CDCl_3$) δC / ppm 156.2, 150.7, 150.1 C^1, 143.7, 141.5, 137.7, 137.4, 137.2, 136.3, 135.8, 135.1, 132.7 C^9, 128.4 C^{14}, 128.4 C^{11}, 128.2 C^{20}, 126.7 C^7, 123.83 C^2, 123.2, 121.7, 21.1 C^{17} and C^{23}, 20.9 C^{22}, 20.7 C^{16}. HRMS (ES^+) *m/z* 470.1476 $[M+H]^+$, calc. 470.1483 for $[C_{29}H_{29}BrN]$.

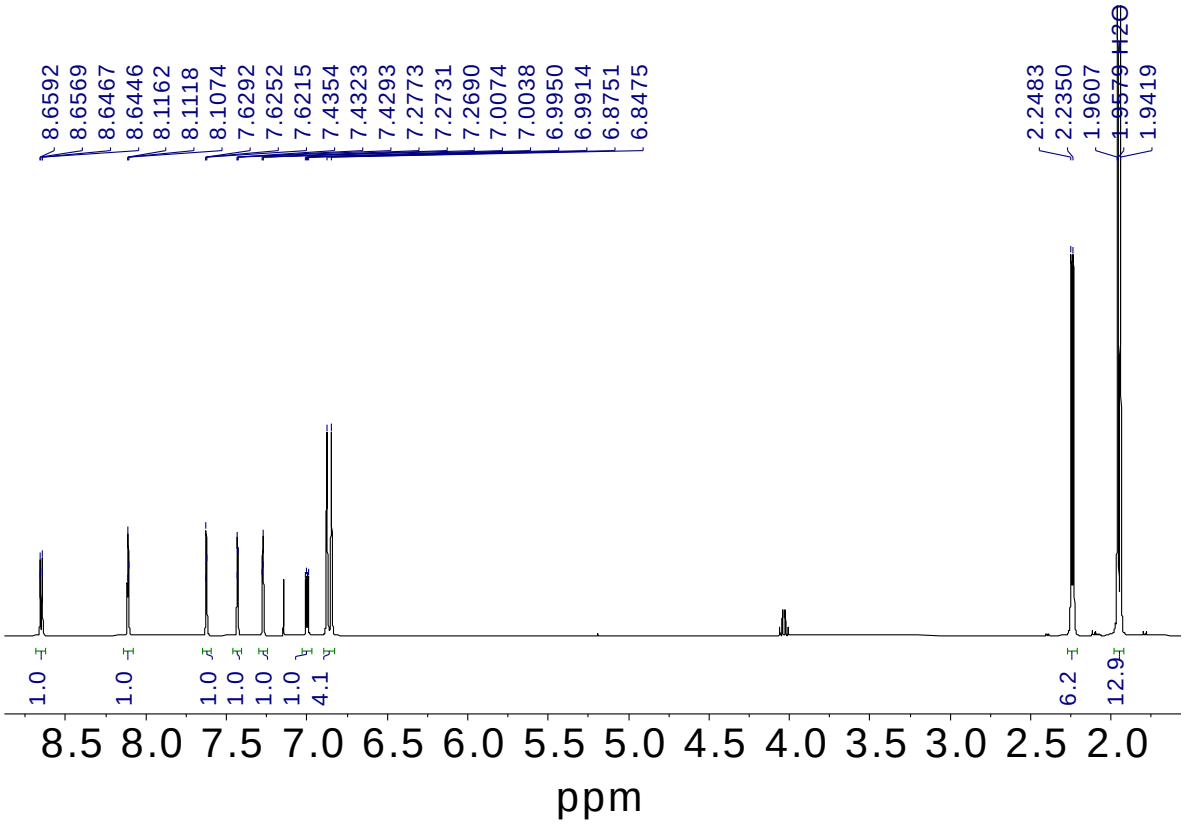

Figure S2.3. ^{1}H NMR spectrum of **2** in $CDCl_3$ at 599 MHz.

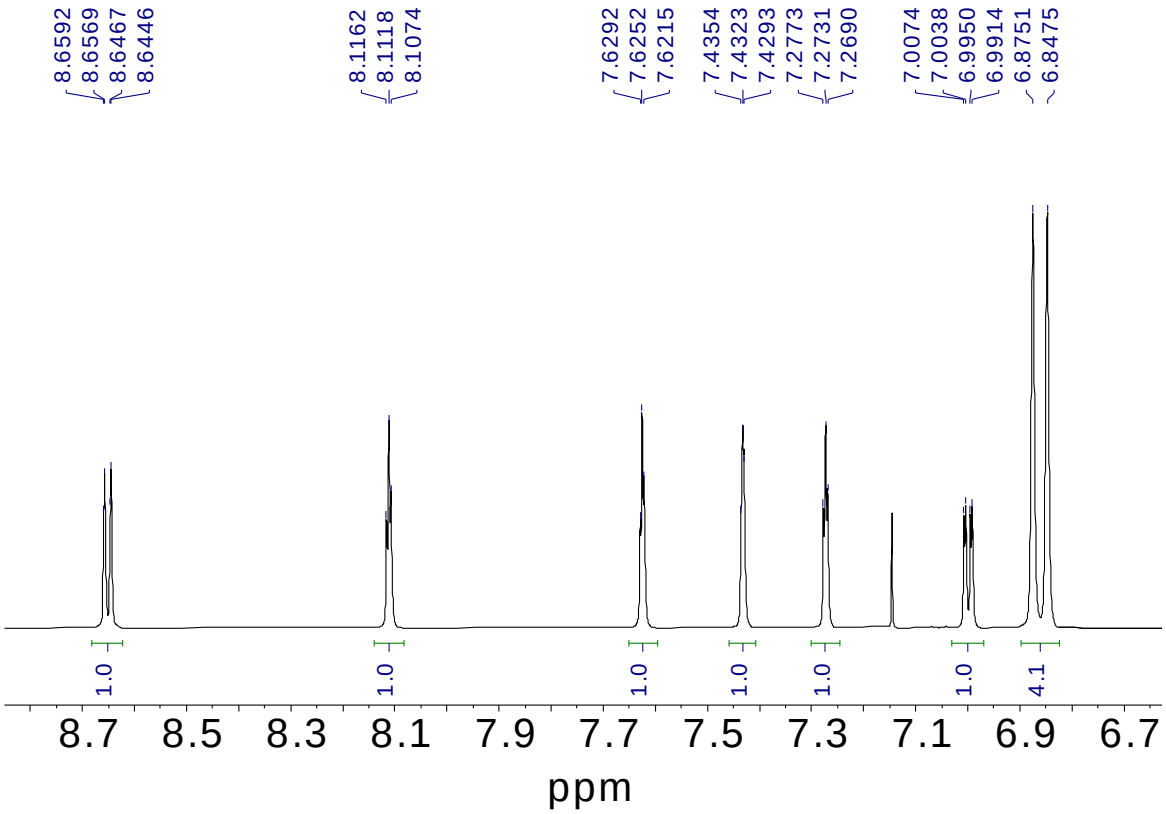

Figure S2.4. ^{1}H NMR spectrum of **2** – aromatic region expanded – in $CDCl_3$ at 599 MHz.

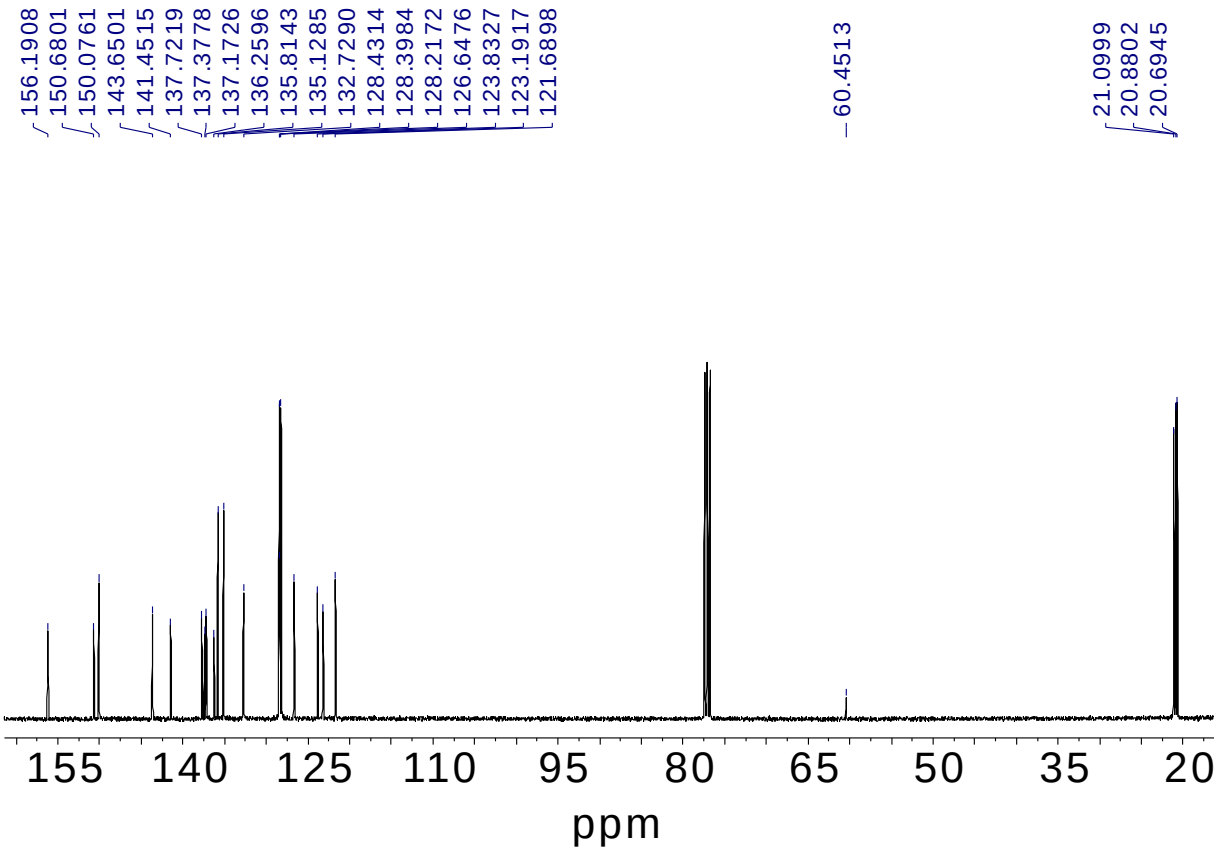

Figure S2.5. ^{13}C NMR spectrum of **2** in $CDCl_3$ at 151 MHz.

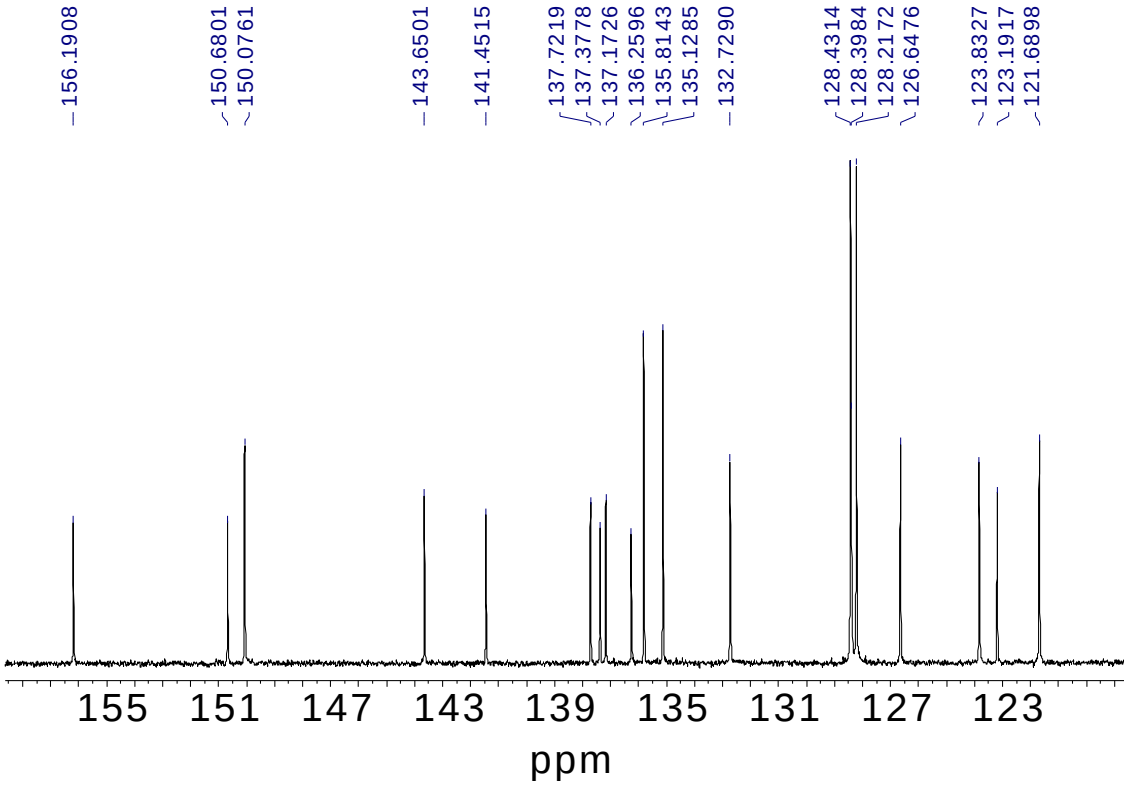

Figure S2.6. ^{13}C NMR spectrum of **2** – aromatic region expanded – in $CDCl_3$ at 151 MHz.

Compound 3

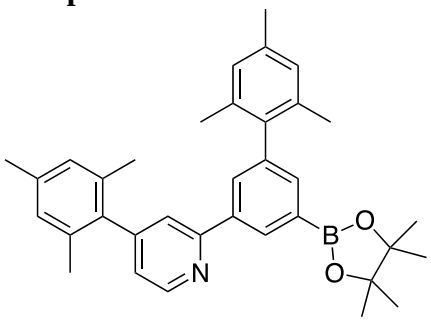

Compound **2** (200 mg, 0.43 mmol), bis(pinacolato)diboron (131 mg, 0.52 mmol), Pd(dppf)Cl_2.CH_2Cl_2 (35 mg, 0.043 mmol), KOAc (0.25 g, 2.58 mmol), and anhydrous 1,4-dioxane (8 mL) were placed in a Schlenk flask. The flask was then evacuated and backfilled with nitrogen five times and heated at 90°C under nitrogen for 18 h. The mixture was then cooled to RT, diluted with 50 mL of deionised water and extracted with CH_2Cl_2 (3 × 30 mL). The extracts were combined, washed first with brine and then deionised water and dried over anhydrous $MgSO_4$. Combined dried extracts were filtered through a plug of silica to remove the catalyst. The filtrate was evaporated down to give a pale-yellow **3** and used without further purification in the next step: TLC (petroleum ether:ethyl acetate 95:5 v/v) showed no starting compound **2** remaining.

Compound 4

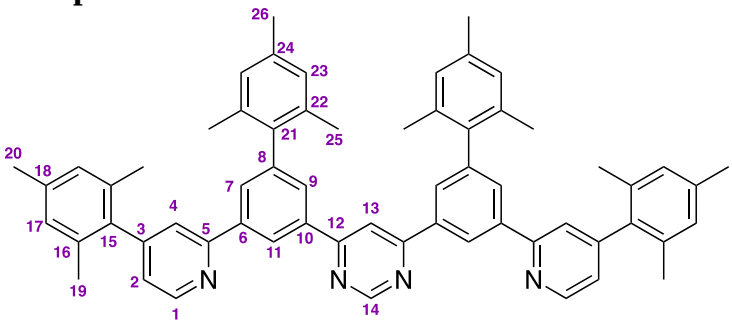

Commercial but impure 4,6-dichloropyrimidine in the form of orange crystals was first dissolved in the minimal volume of CH_2Cl_2 and the solution was filtered through a plug of silica. The solvent was removed from the filtrate under reduced pressure to give the starting material as white crystals. This material (15 mg, 0.10 mmol) was placed in a Schlenk flask with the crude pinacol ester **3** (113 mg, 0.22 mmol), $Pd(PPh_3)_4$ (20 mg, 0.017 mmol), Cs_2CO_3 (0.63 g, 1.9 mmol), and anhydrous toluene (5 mL). The mixture was then evacuated and backfilled with nitrogen five times and heated to 90°C under nitrogen for 18 h. The mixture was then cooled to RT, diluted with 20 mL of deionised water and extracted with CH_2Cl_2

(6 × 25 mL), noting the only modest solubility of **4** in dichloromethane. The extracts were combined, washed with more deionised water and dried with anhydrous $MgSO_4$ and filtered. The CH_2Cl_2 solutions were concentrated using a rotary evaporator to a volume of approx. 10 mL at which stage an equal amount of acetone was added to aid precipitation of the product **4**, followed by evaporation of the remaining solvent mixture to near-dryness. The off-white precipitate was washed with acetone and redissolved in chloroform. An equal amount of acetone was then added to the chloroform solution and the mixture was evaporated to dryness. The cycle of precipitation and redissolution was performed a total of three times, after which the product was assessed to be of sufficient purity. The precipitate was then dried under vacuum. This procedure gave **4** in form of a white powder (30 mg, 35%). Further preparations gave **4** on a similar scale.

^{1}H NMR (599 MHz, $CDCl_3$) δH / ppm 9.34 (1 H, d, J 1.5, H^{14}), 8.87 (2 H, br s, H^{11}), 8.78 (2 H, d, J 5.0, H^1), 8.30 (1 H, br s, H^{13}), 8.01 – 7.96 (4H, m, H^9 and H^7), 7.67 (2 H, br s, H^4), 7.11 (2 H, d, J 5.0, H^2), 6.98 – 6.96 (8 H, m, H^{17} and H^{23}), 2.36 – 2.32 (12 H, m, H^{20} and H^{26}), 2.09 (12 H, s, H^{25}), 2.05 (12 H, s, H^{19}). ^{13}C NMR (176 MHz, $CDCl_3$) δC / ppm 164.5 C^{12}, 159.2 C^{14}, 150.0 C^1, 138.1, 137.8, 137.6, 137.0, 135.9, 135.1, 130.4 C^7, 128.7 C^9, 128.4 C^{17} or C^{23}, 128.2 C^{17} or C^{23}, 124.3 C^{11}, 123.6 C^2, 121.8 C^4, 113.1 C^{13}, 21.1 C^{20} and C^{26}, 21.0 C^{25}, 20.7 C^{19}. HRMS (ES^+) *m/z* 859.4728 $[M+H]^+$, calc. 859.4740 for $[C_{62}H_{59}N_4]$.

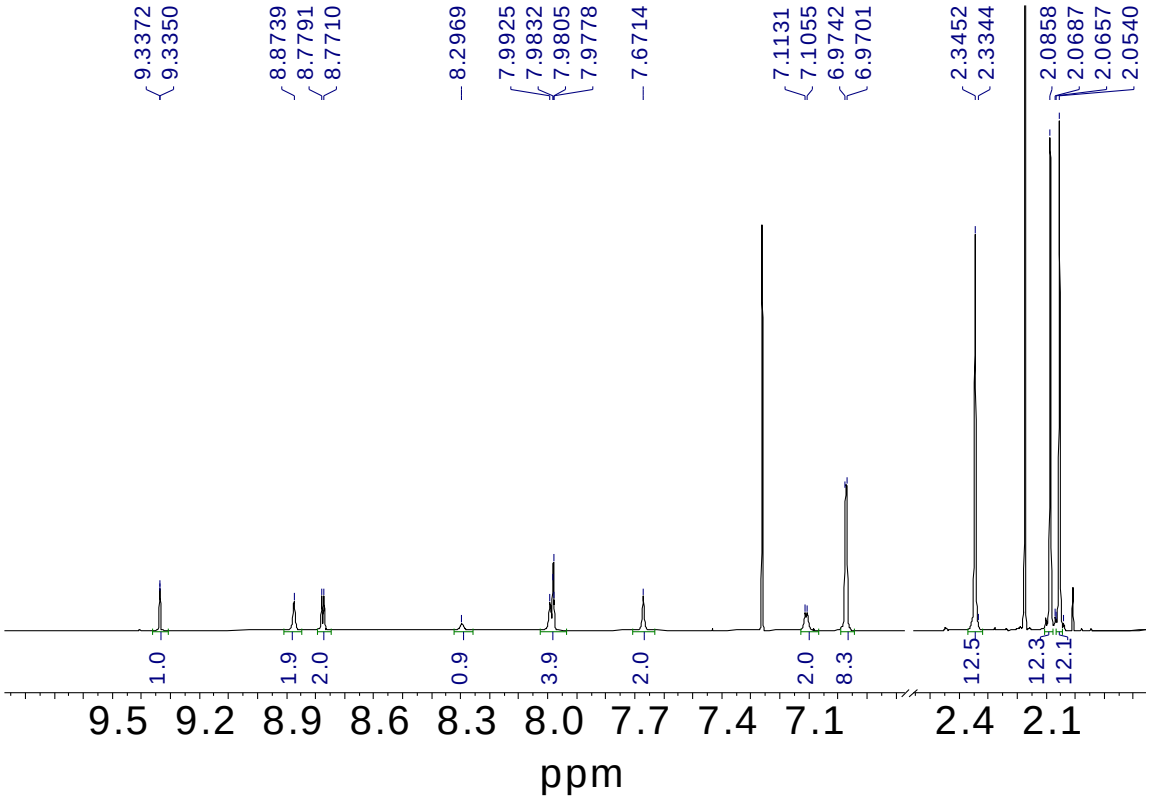

Figure S2.7. ^{1}H NMR spectrum of **4** in $CDCl_3$ at 599 MHz.

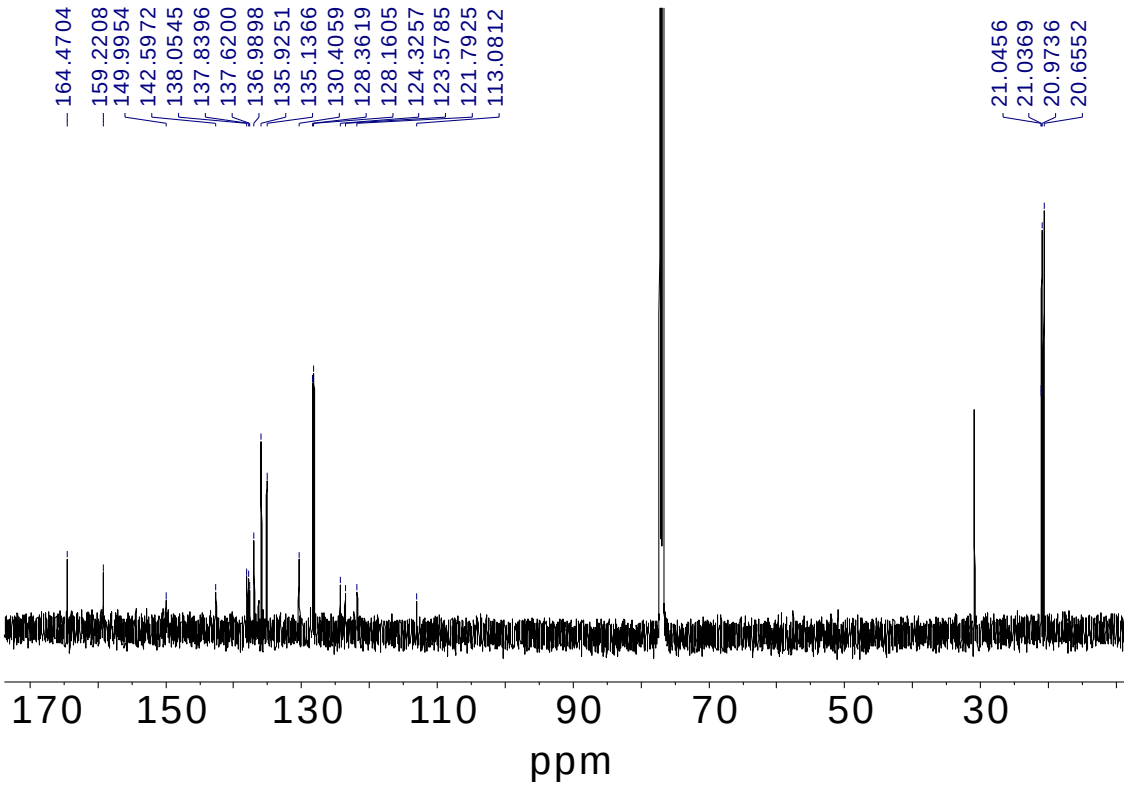

Figure S2.8. ^{13}C NMR spectrum of **4** in $CDCl_3$ at 151 MHz.

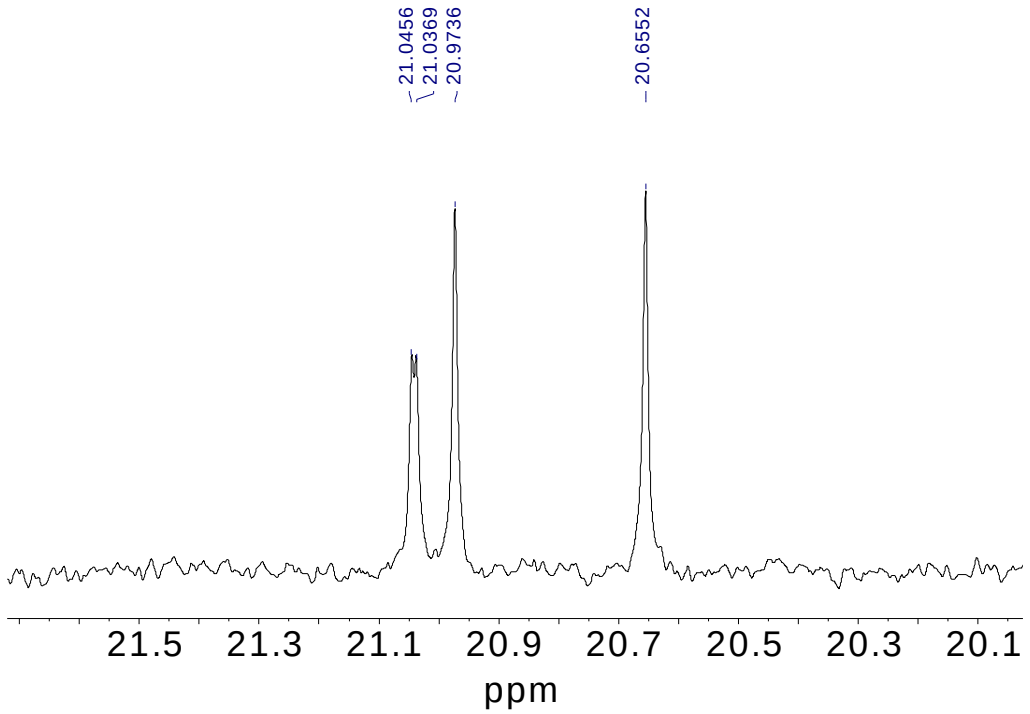

Figure S2.9. ^{13}C NMR spectrum of **4** –aliphatic region expanded – in $CDCl_3$ at 151 MHz.

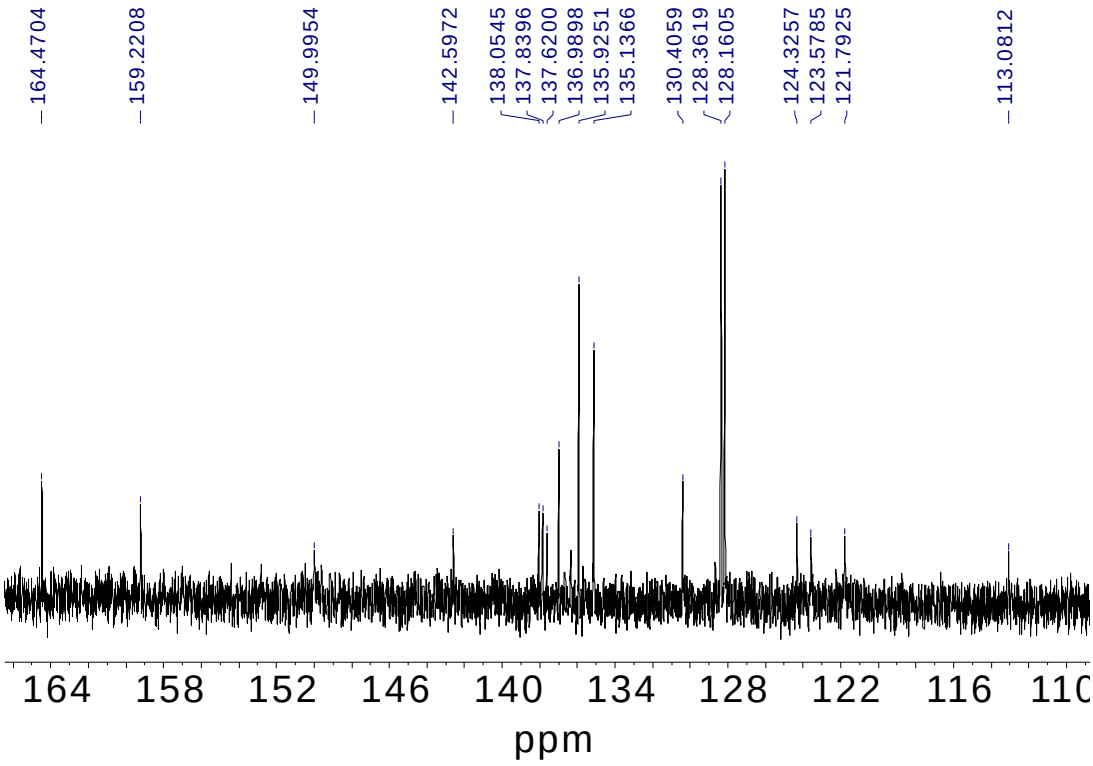

Figure S2.10. ^{13}C NMR spectrum of **4** –aromatic region expanded – in $CDCl_3$ at 151 MHz.

Compound 5: L(Pt–Cl)$_2$

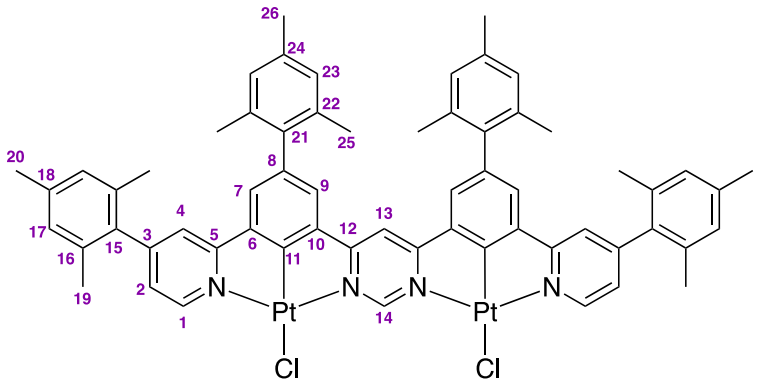

K_2PtCl_4 (33 mg, 0.079 mmol) and **4** (31 mg, 0.036 mmol) were dissolved in acetic acid (5 mL) and degassed by three freeze-pump-thaw cycles. The mixture was heated at reflux for 24 h. After cooling, water (5 mL) was added. The resulting precipitate was isolated and washed with water (20 mL). The product was dried under reduced pressure and purified by gradient column chromatography on silica with hexane : ethyl acetate (100 : 0 to 70 : 30) to yield a red solid (31 mg, 65% yield).

^{1}H NMR (700 MHz, $CDCl_3$) δH / ppm 10.59 (1H, d, J 1.0, H^{14}), 9.41 (2H, d, J 6.0, H^1), 7.72 (1H, s, H^{13}), 7.42 – 7.39 (2H, m, H^4), 7.37 (2H, d, J 1.0, H^9), 7.29 (2H, d, J 1.0, H^7), 7.12 (2H, dd, J 6.0, 2.0, H^2), 6.90 (4H, s, H^{17}), 6.86 (4H, s, H^{23}), 2.27 (6H, s, H^{20}), 2.25 (6H, s, H^{26}), 2.00 (12H, s, H^{19}), 1.99 (12H, s, H^{25}) ^{13}C NMR (176 MHz, $CDCl_3$) δC / ppm 175.4, 166.7, 165.3, 162.4 C^{14}, 154.0, 152.3 C^1, 142.3, 138.5, 137.9, 137.8, 137.2, 136.7, 135.7, 134.9, 134.7, 128.7 C^{17}, 128.7 C^7, 128.3 C^{23}, 127.4 C^9, 125.2 C^2, 120.9 C^4, 108.0 C^{13}, 21.1 C^{20}, 21.1 C^{26}, 21.0 C^{25}, 20.7 C^{19}

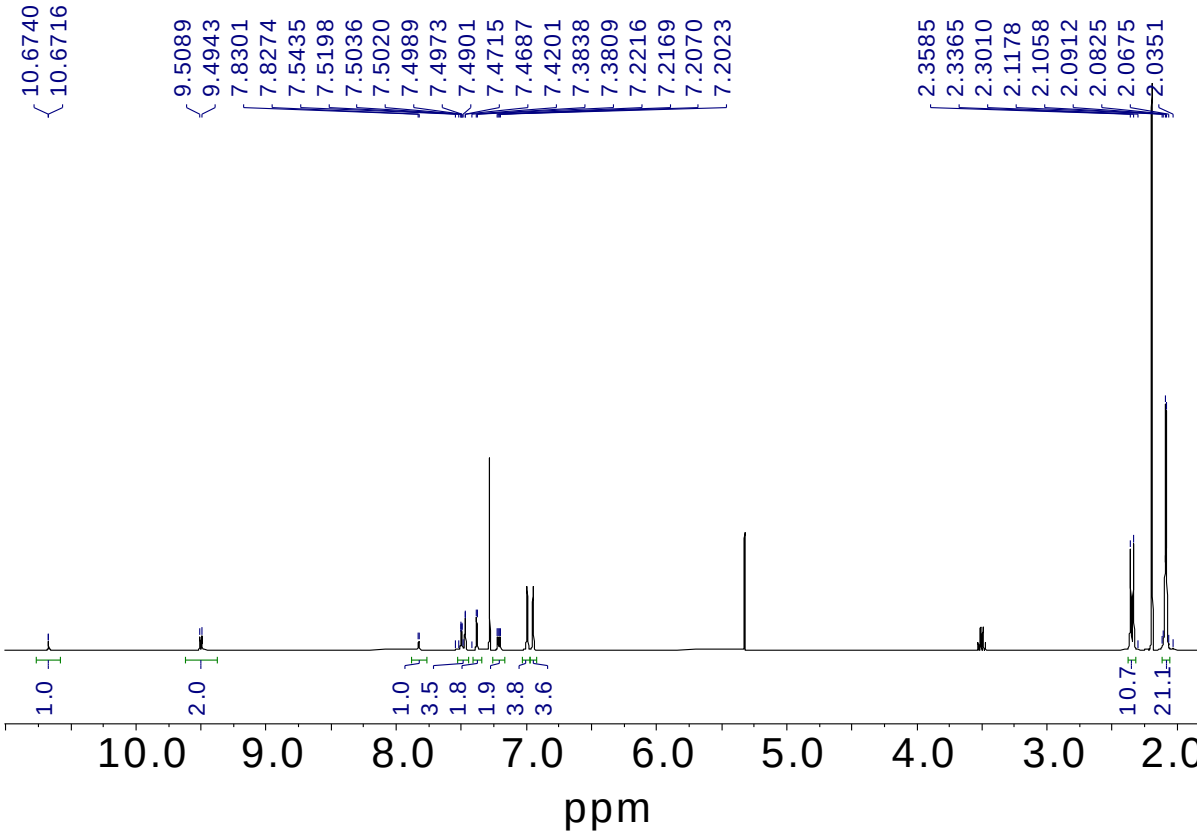

Figure S2.11. ^{1}H NMR spectrum of **5** $CDCl_3$ at 400 MHz.

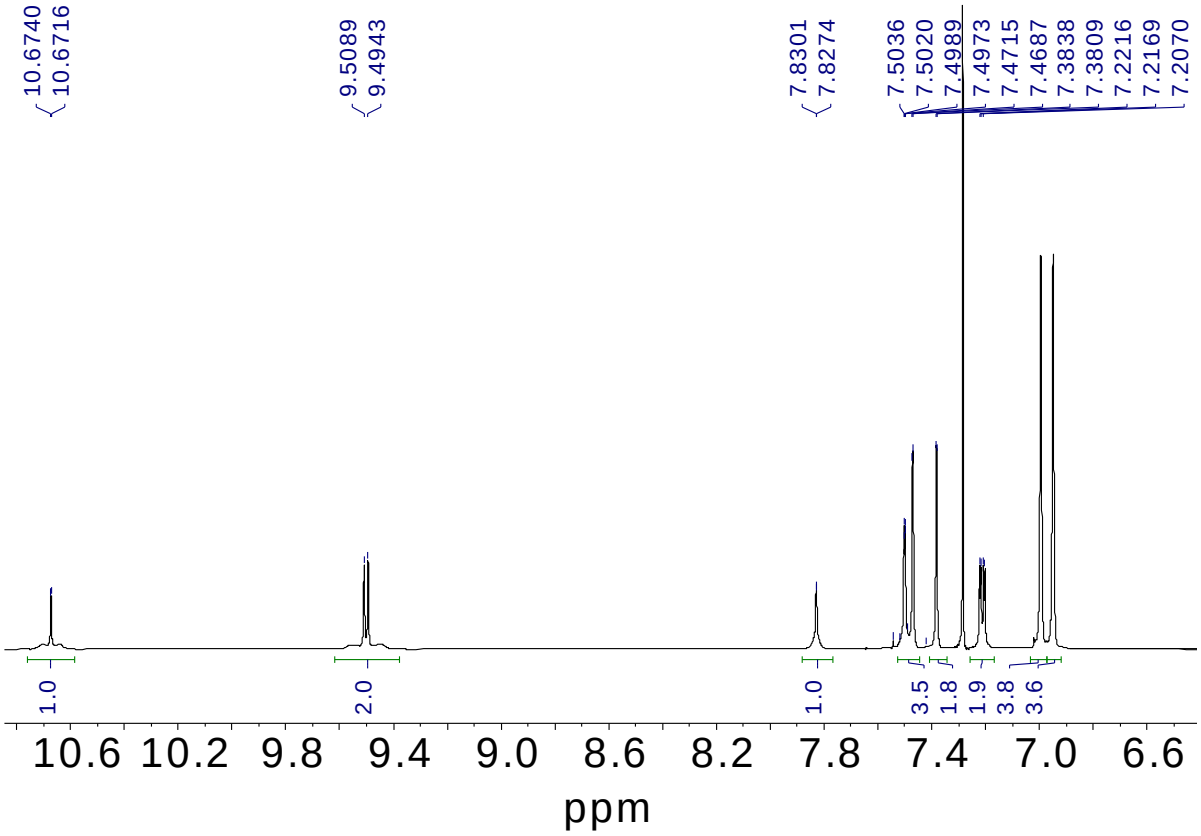

Figure S2.12. ^{1}H NMR spectrum of **5 –** aromatic region expanded – in $CDCl_3$ at 400 MHz.

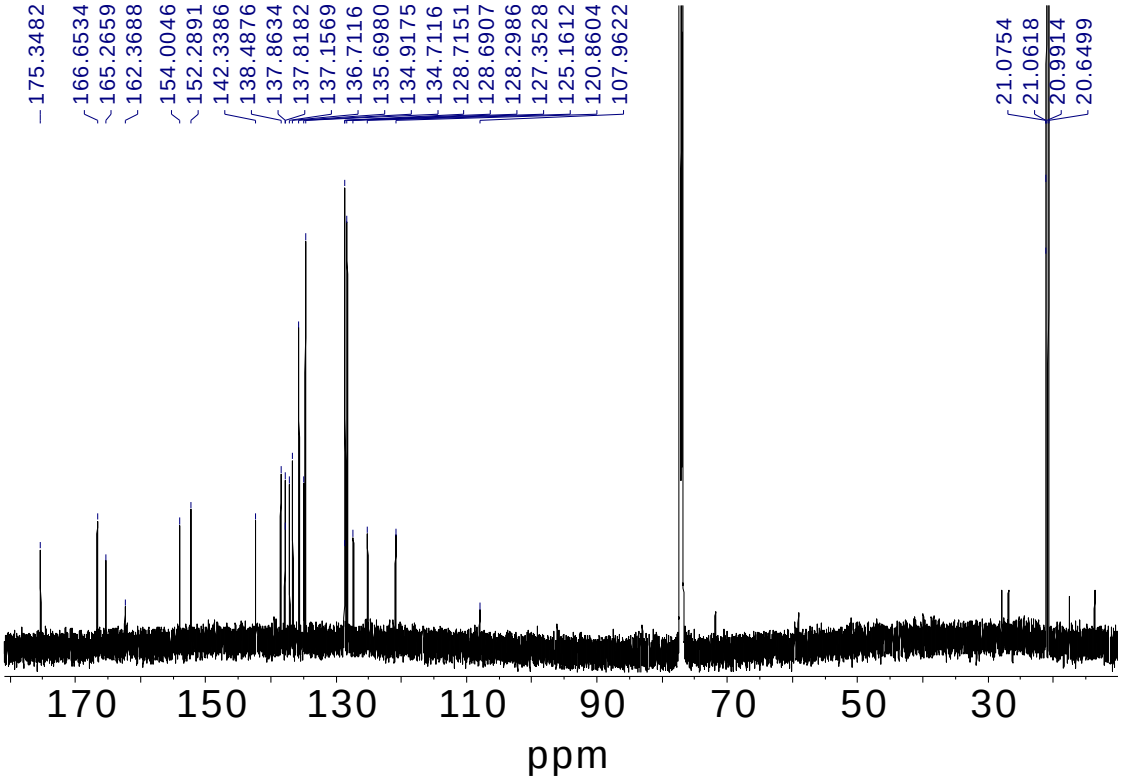

Figure S2.13. ^{13}C NMR spectrum of **5** in $CDCl_3$ at 176 MHz.

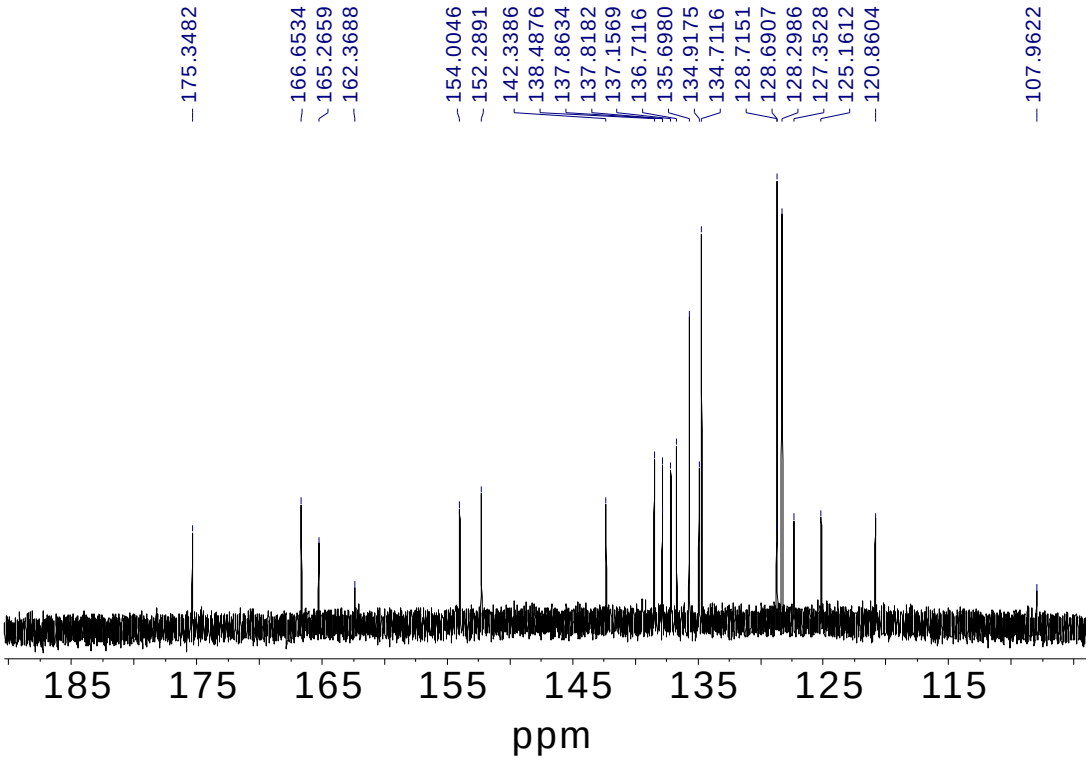

Figure S2.14. ^{13}C NMR spectrum of **5 –** expanded aromatic region – in $CDCl_3$ at 176 MHz.

Compound 6: L(Pt–I)$_2$

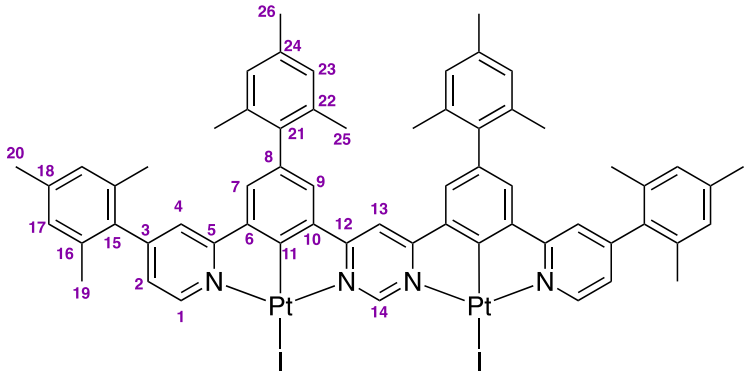

Compound **5** (15 mg, 0.011 mmol) and AgOTf (7 mg, 0.028 mmol) were suspended in acetone and the mixture stirred at ambient temperature for 90 minutes. The AgCl that precipitated was removed from the solution by centrifugation. KI (5 mg, 0.028 mmol) was added to the acetone solution and stirred at ambient temperature for 2 h. The solvent was removed and the product purified by gradient column chromatography on silica with hexane : ethyl acetate (100 : 0 to 80 : 20) to yield a dark red solid (11 mg, 67% yield).

^{1}H NMR (599 MHz, $CDCl_3$) δH / ppm 11.60 (1H, s, H^{14}), 10.00 (2H, d, J 6.0, H^{1}), 7.75 – 7.74 (1H, m, H^{13}), 7.45 (2H, d, J 2.0, H^{4}), 7.43 (2H, d, J 1.0, H^{9}), 7.36 (2H, d, J 1.0, H^{7}), 7.11 (2H, dd, J 6.0, 2.0, H^{2}), 6.96 (4H, s, H^{17}), 6.91 (4H, s, H^{23}), 2.32 (6H, s, H^{20}), 2.30 (6H, s, H^{26}), 2.05 (12H, s, H^{19}), 2.04 (12H, s, H^{25}) ^{13}C NMR (151 MHz, $CDCl_3$) δC / ppm 174.0, 172.4 C^{14}, 166.1, 164.4, 157.1 C^{1}, 153.7, 142.4, 138.5, 138.0, 137.6, 137.2, 137.0, 135.6, 134.7, 134.7, 128.9 C^{7}, 128.7 C^{17}, 128.3 C^{23}, 127.3 C^{9}, 125.8 C^{2}, 121.0 C^{4}, 107.9 C^{13}, 21.0 C^{20}, 21.0 C^{26}, 21.0 C^{25}, 20.6 C^{1}.

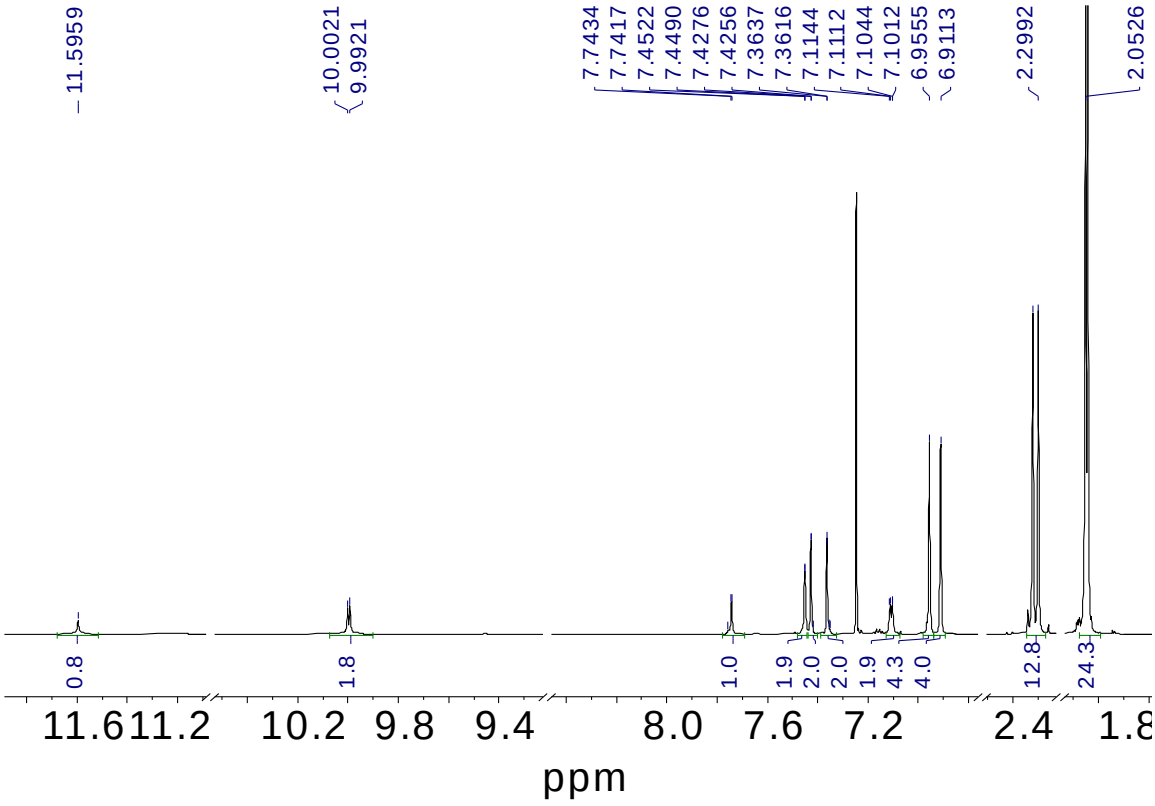

Figure S2.15. ^{1}H NMR spectrum of **6** in $CDCl_3$ at 599 MHz.

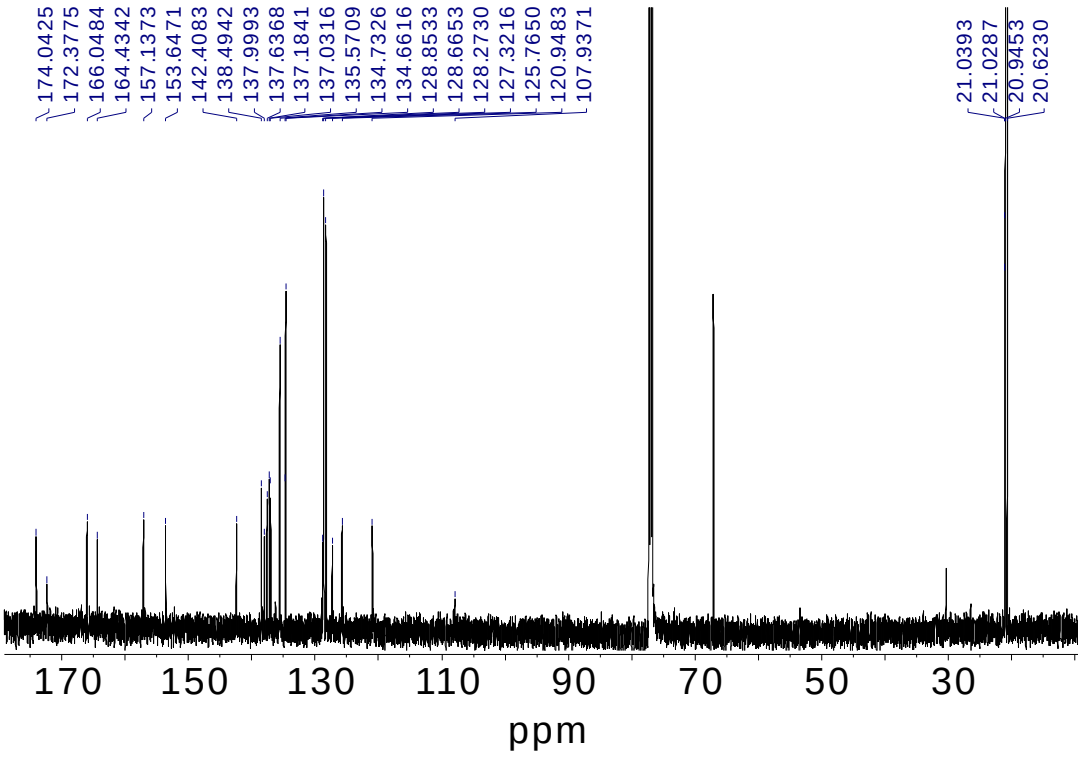

Figure S2.16. ^{13}C NMR spectrum of **6** in $CDCl_3$ at 151 MHz.

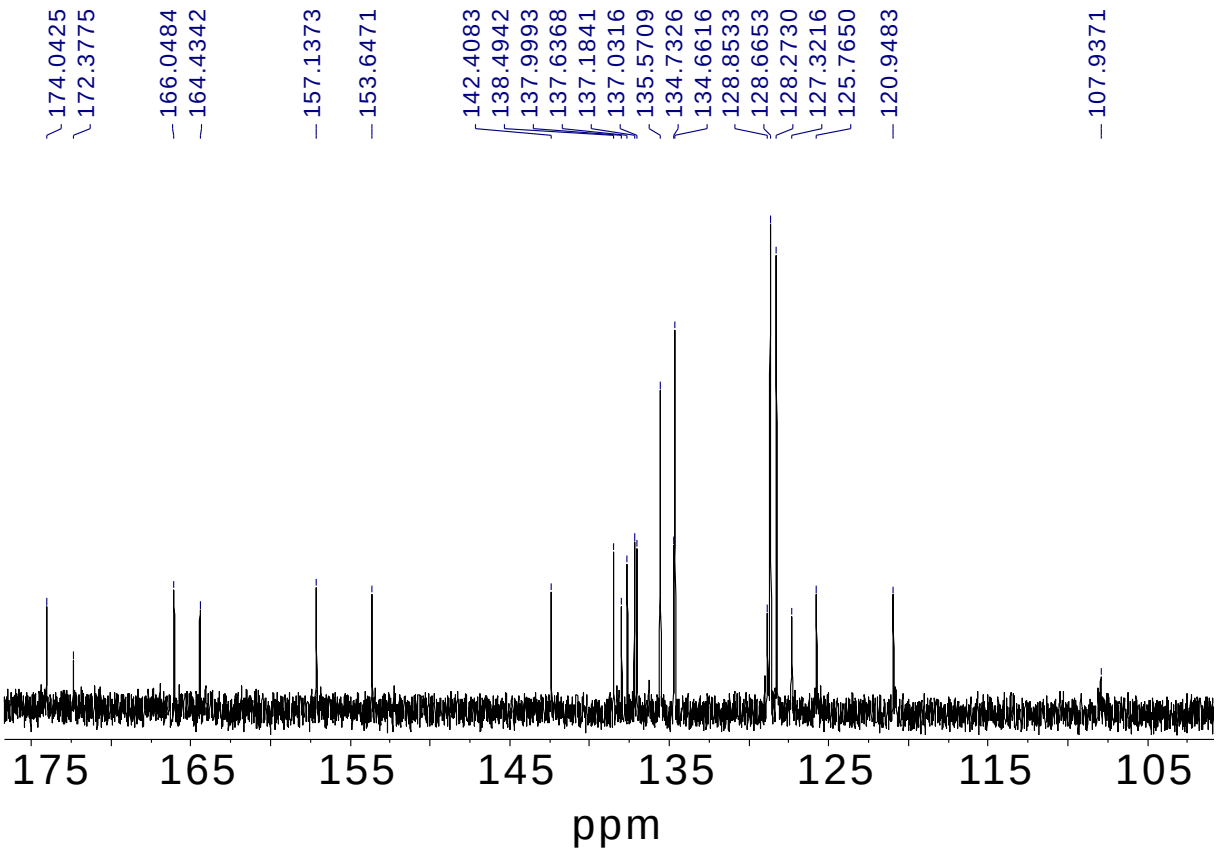

Figure S2.17. ^{13}C NMR spectrum of **6** – expanded aromatic region – in $CDCl_3$ at 151 MHz.

Compound 7: L(Pt–Cl_3)$_2$

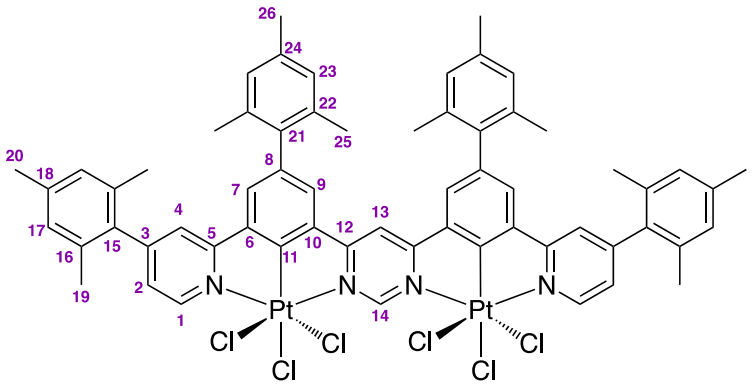

Compound 5 (7 mg, 0.005 mmol) and $PhICl_2$ (3 mg, 0.010 mmol) were dissolved in $CHCl_3$ (7 mL) and the mixture was stirred for 18 h with the partial exclusion of light. The solvent was removed under reduced pressure and the resulting solid washed with diethyl ether (15 mL), extracted into DCM, and the solvent removed under reduced pressure to yield the product as a dark yellow solid (6 mg, 78% yield).

^{1}H NMR (400 MHz, $CDCl_3$) δH / ppm 10.77 (1H, s, H^{14}), 9.63 (2H, d, J 6.0, H^1), 8.35 (1H, s, H^{13}), 7.83 (2H, s, H^9 or H^7), 7.71 (2H, d, J 2.0, H^4), 7.68 (2H, s, H^9 or H^7), 7.43 (2H, dd, J 6.0, 2.0, H^2), 7.02 (4H, s, H^{17} or H^{23}), 6.99 (4H, s, H^{17} or H^{23}), 2.37 (6H, s, H^{20} or H^{26}), 2.36 (6H, s, H^{20} or H^{26}), 2.11 (12H, s, H^{19} or H^{25}), 2.09 (12H, s, H^{19} or H^{25}). ^{13}C NMR (151 MHz, $CDCl_3$) δC / ppm 152.3 C^1, 132.4 C^9 or C^7, 130.4 C^9 or C^7, 129.3 C^{17} or C^{23}, 128.5 C^{17} or C^{23}, 127.3 C^2, 123.6 C^4, 21.1 C^{20}, 21.1 C^{26}, 21.1 C^{19} or C^{25}, 20.9 C^{19} or C^{25}. The identity of the material was confirmed by X-ray on a crystal obtained from a solution of the compound in acetone: see Section 3.

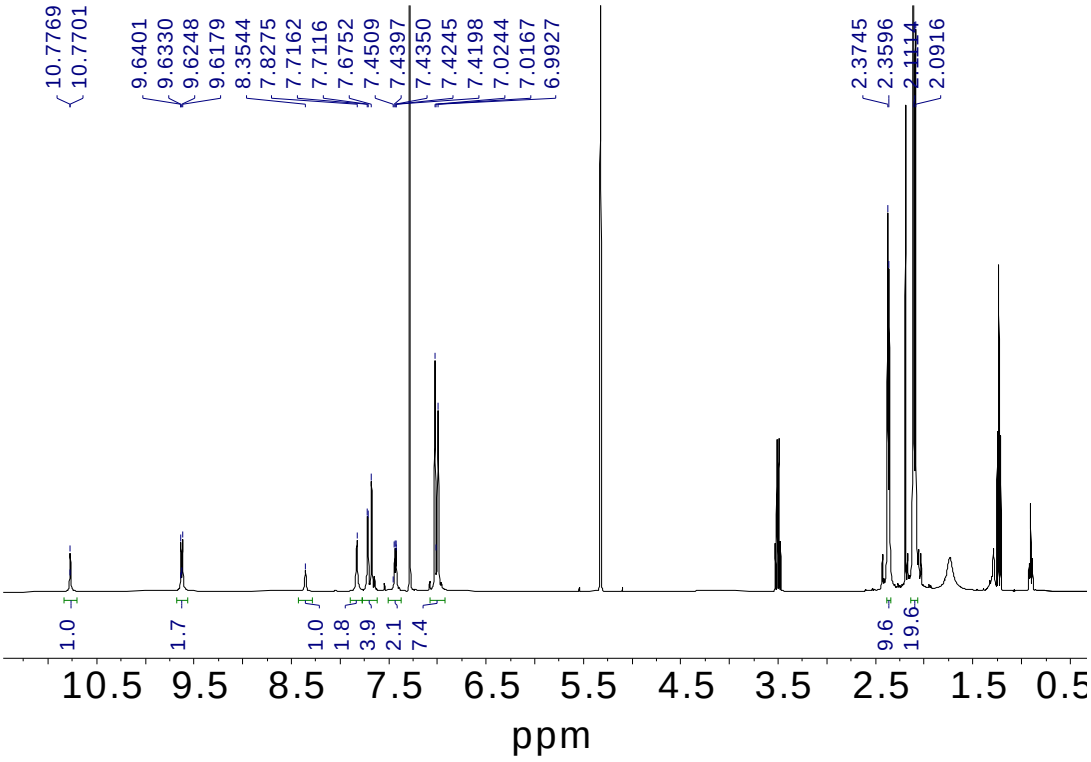

Figure S2.18. ^{1}H NMR spectrum of **7** in $CDCl_3$ at 400 MHz.

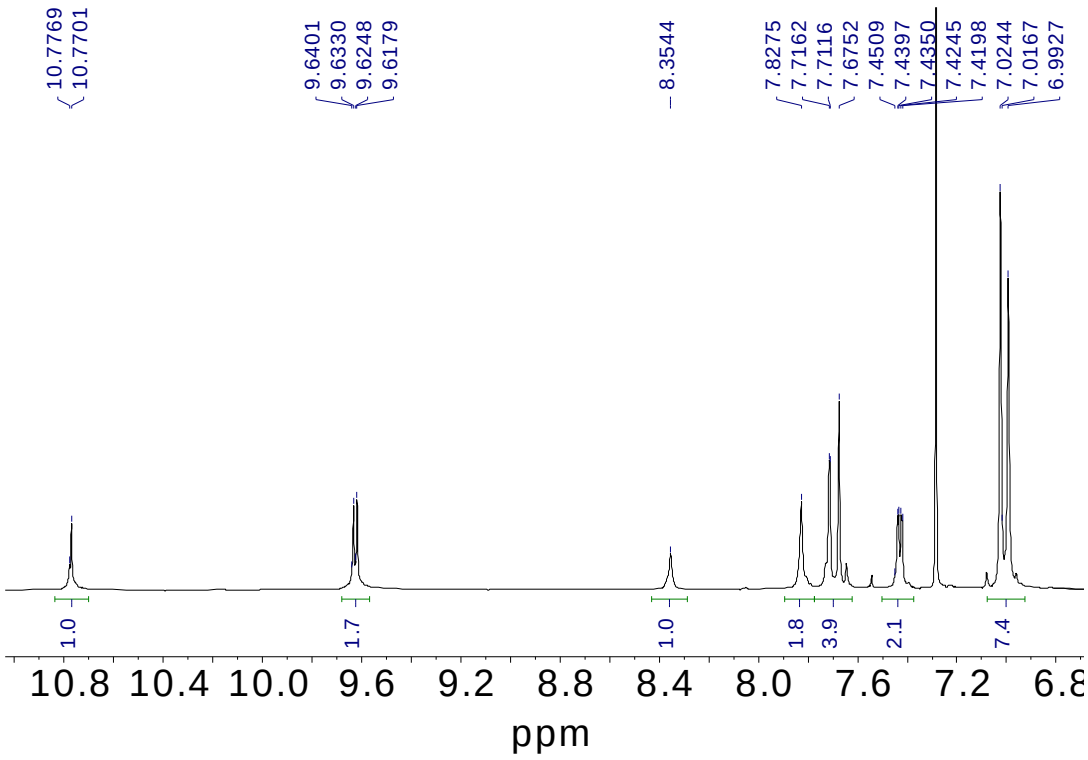

Figure S2.19. ^{1}H NMR spectrum of **7** – expanded aromatic region – in $CDCl_3$ at 400 MHz.

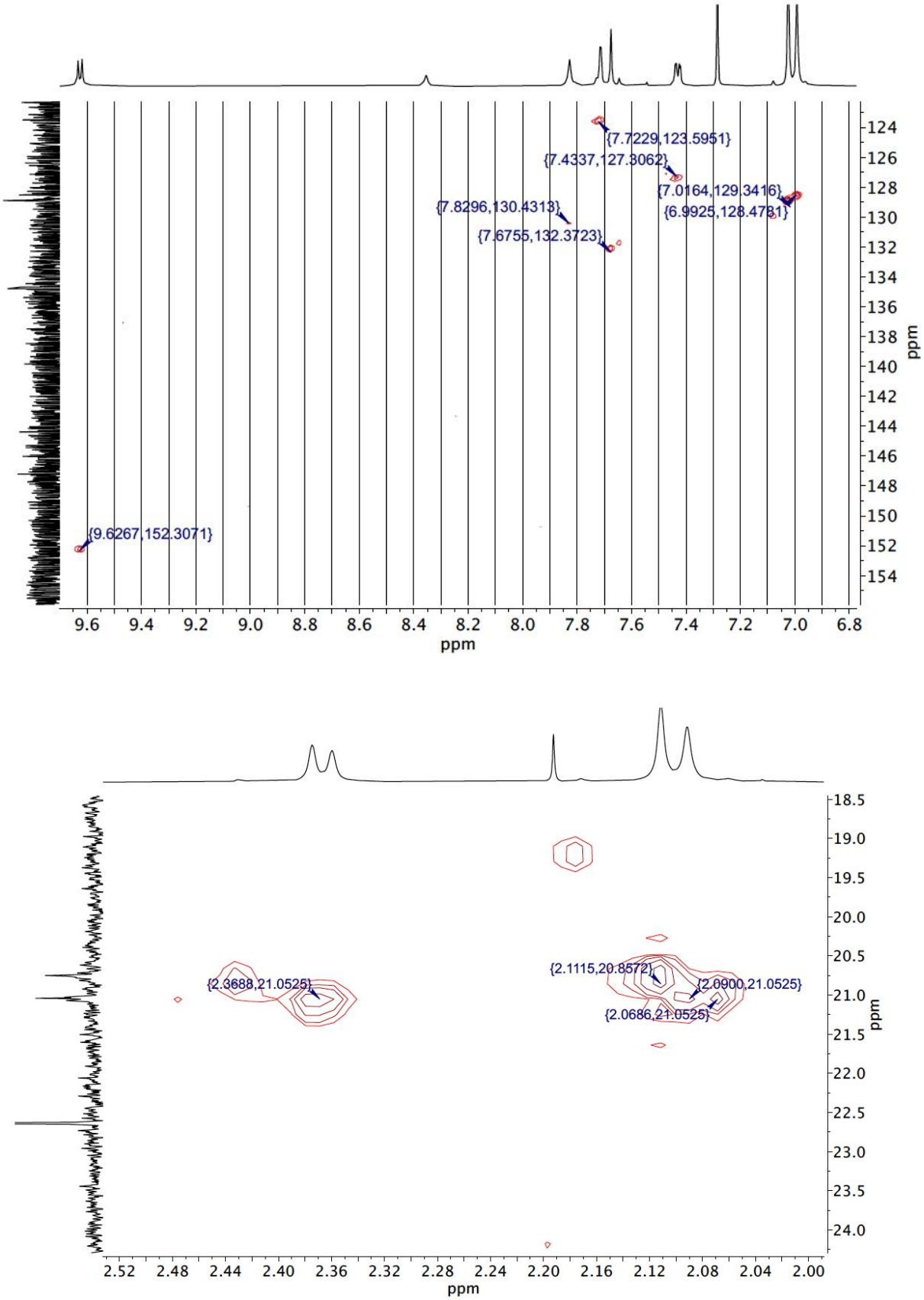

Figure S2.20. ^{1}H–^{13}C HSQC spectrum of **7** in $CDCl_3$: aromatic (top) and aliphatic (bottom) regions.

3. Crystallography

The X-ray single crystal data for compound **7** have been collected using λMoKα radiation (λ =0.71073Å) on a Bruker D8Venture (Photon III MM C14 CPAD detector, IμS-III-microsource, focusing mirrors) 3-circle diffractometer equipped with a Cryostream (Oxford Cryosystems) open-flow nitrogen cryostat at the temperature 120.0(2)K. The structure was solved by direct method and refined by full-matrix least squares on F^2 for all data using Olex2[18] and SHELXTL[19] software. All non-hydrogen atoms were refined in anisotropic approximation; hydrogen atoms were placed in the calculated positions and refined in riding mode. Disordered atoms of the mesityl groups were refined with fixed SOF=0.5. The structure contains a number of severely disordered acetone solvent molecules. Some of them could not be properly located and refined. Their contribution (42 e, appr.1.5 C_3H_6O) to the structural factors was taken into account by applying MASK procedure of OLEX2 program package. Crystal data and parameters of refinement are listed in Table S.3.1 below. Crystallographic data for the structure have been deposited with the Cambridge Crystallographic Data Centre as supplementary publication CCDC-2365020.

Table S3.1. Crystal data and structure refinement for complex **7.**

Identification code	23srv209
Empirical formula	$C_{69.5}H_{71}Cl_6N_4O_{2.5}Pt_2$
Formula weight	1605.18
Temperature/K	120.00
Crystal system	triclinic
Space group	P-1
a/Å	11.9989(3)
b/Å	15.3185(4)
c/Å	21.3676(5)
α/°	74.3417(9)
β/°	85.7026(10)
γ/°	71.9046(9)
Volume/Å^3	3594.51(16)
Z	2
ρ_{calc}g/cm^3	1.483
μ/mm^{-1}	4.155
F(000)	1588.0
Crystal size/mm^3	0.11 × 0.04 × 0.02
Radiation	Mo Kα (λ = 0.71073)
2Θ range for data collection/°	3.912 to 59.998
Index ranges	$-16 \leq h \leq 16$, $-21 \leq k \leq 21$, $-30 \leq l \leq 30$
Reflections collected	131810
Independent reflections	20946 [R_{int} = 0.0824, R_{sigma} = 0.0607]
Data/restraints/parameters	20946/232/874
Goodness-of-fit on F^2	1.043
Final R indexes [I>=2σ (I)]	R_1 = 0.0519, wR_2 = 0.0999
Final R indexes [all data]	R_1 = 0.0779, wR_2 = 0.1088
Largest diff. peak/hole / e Å^{-3}	1.51/-3.30

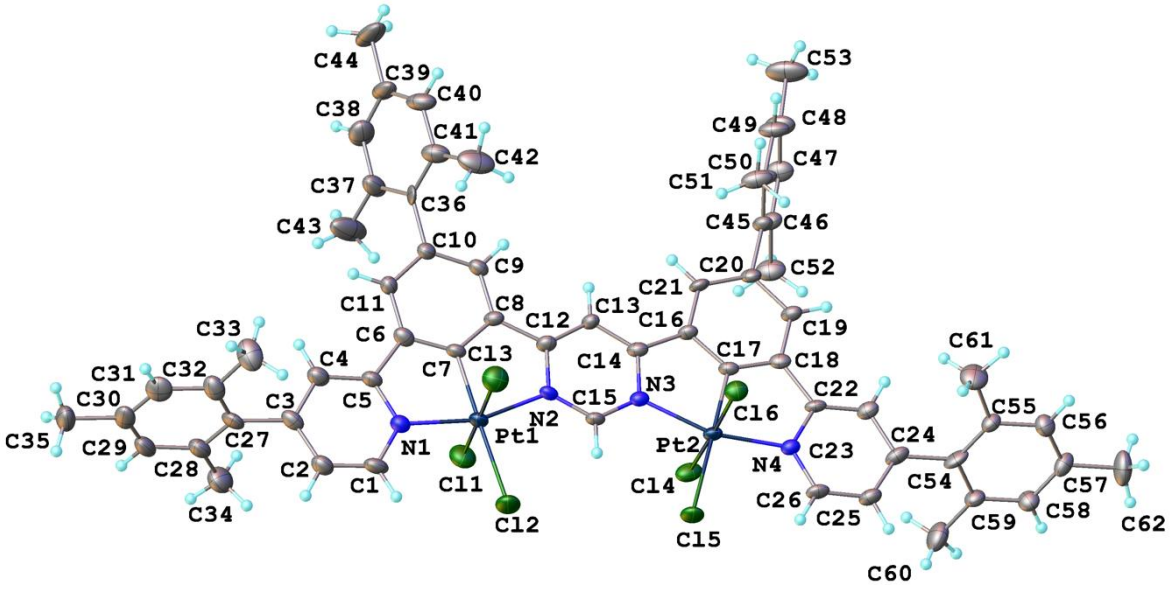

Figure S3.1. Molecular structure of **7** in the crystal, determined by X-ray diffraction at 120 K.

Table S3.2. Selected bond lengths (Å) and angles (°) for compound **7** (*pym* denotes the pyrimidine ring, *pyr* denotes a pyridine).

	bond length / Å		**bond angle / °**
Pt^1–C	1.942(5)	Cl^1–Pt^1–Cl^3	177.19(6)
Pt^1–N^{pym}	2.032(4)	N^{pym}–Pt^1–N^{pyr}	161.23(17)
Pt^1–N^{pyr}	2.031(5)	C–Pt^1–$Cl^{trans\text{-}to\text{-}C}$	178.26(16)
Pt^1–$Cl^{trans\text{-}to\text{-}C}$	2.4166(14)	Cl^4–Pt^2–Cl^6	177.11(5)
Pt^1–Cl^1	2.3017(17)	N^{pym}–Pt^2–N^{pyr}	161.31(17)
Pt^1–Cl^3	2.3217(17)	C–Pt^2–$Cl^{trans\text{-}to\text{-}C}$	179.11(16)
Pt^2–C	1.941(5)		
Pt^2–N^{pym}	2.047(4)		
Pt^2–N^{pyr}	2.027(4)		
Pt^2–$Cl^{trans\text{-}to\text{-}C}$	2.4327(13)		
Pt^2–Cl^4	2.3054(14)		
Pt^2–Cl^6	2.3197(14)		

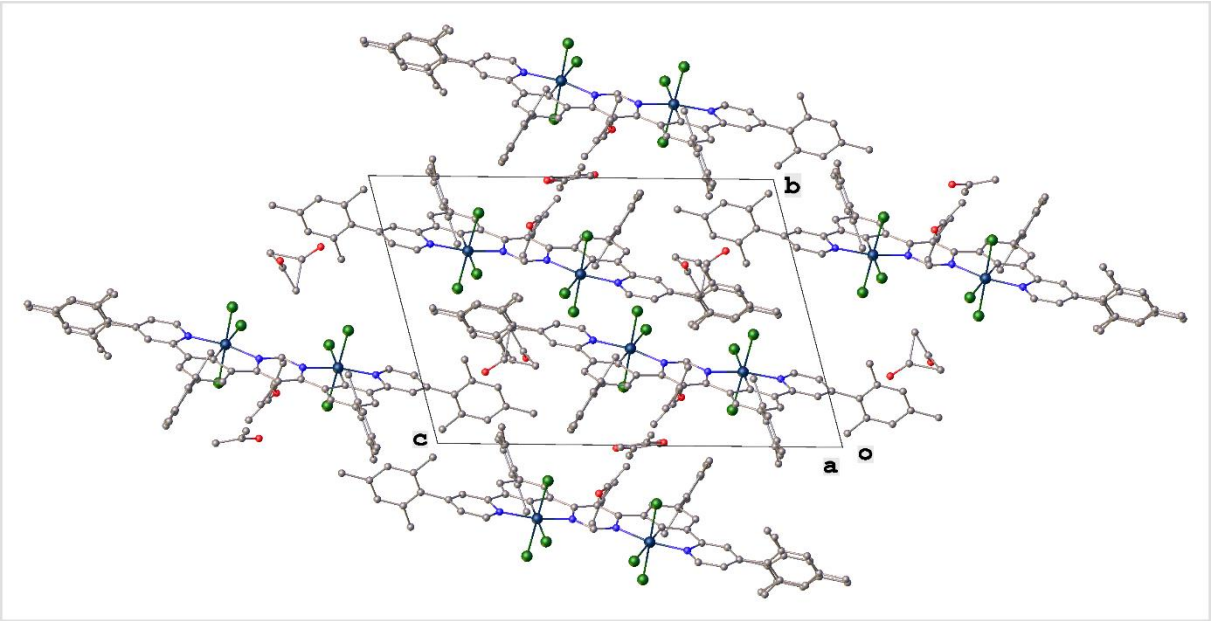

Figure S3.2. The packing of molecules of **7** in the crystal.

4. Computations

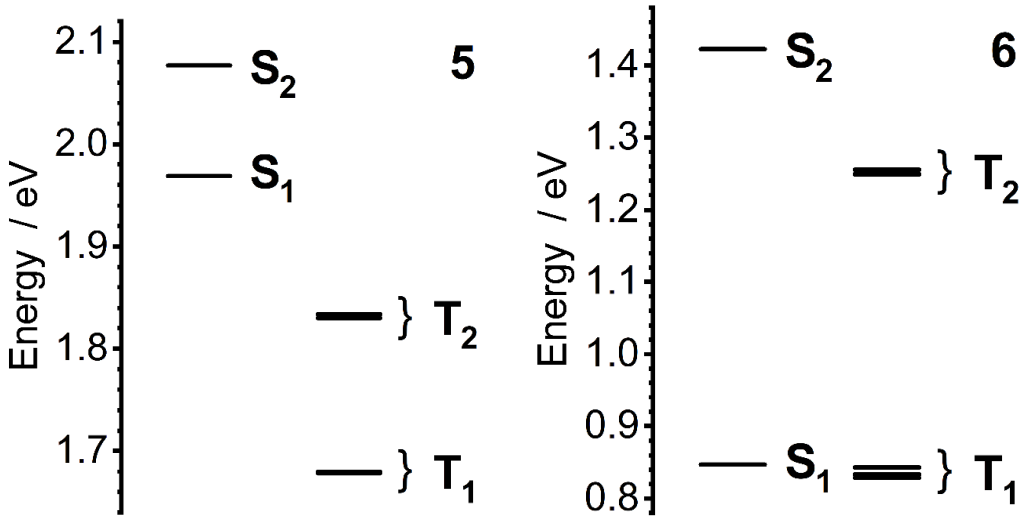

Figure S4.1. Calculated energy-level diagram of singlet and triplet excited states of complexes **5** and **6** at the T_1 geometry.

Table S4.1. Composition of the relevant SOC states in complex **5** at T_1 geometry.

Complex	State	Energy / eV	*f*	Contribution of zero-order states*
5	1	1.6782	4.7×10^{-7}	T_1 (89.1%)
	2	1.6790	8.0×10^{-8}	T_1 (88.9%)
	3	1.6798	2.0×10^{-4}	T_1 (89.3%)
	4	1.8298	2.7×10^{-3}	T_2 (87.7%)
	5	1.8332	2.6×10^{-7}	T_2 (87.6%)
	6	1.8337	1.4×10^{-4}	T_2 (87.8%)
	7	1.9689	0.20	S_1 (68.0%), T_3 (20.8%), T_4 (5.3%)
	8	2.0767	4.7×10^{-3}	S_2 (68.7%), T_5 (12.9%), T_9 (10.4%)

* Triplet states with contributions < 5% are not shown.

Table S4.2. Composition of the relevant SOC states in complex **6** at T_1 geometry.

Complex	State	Energy / eV	*f*	Contribution of zero-order states*
6	1	0.8285	3.4×10^{-5}	T_1 (84.7%)
	2	0.8335	1.4×10^{-4}	T_1 (83.3%), S_1 (2.2%)
	3	0.8433	2.0×10^{-3}	T_1 (87.1%), S_4 (7.9%)
	4	0.8470	3.4×10^{-3}	S_1 (81.4%), T_3 (11.7%)
	5	1.2488	2.3×10^{-4}	T_2 (82.4%), T_6 (5.7%), T_3 (5.0%), S_8 (2.8%)
	6	1.2495	4.6×10^{-5}	T_2 (83.0%), T_3 (5.1%), S_6 (6.4%)
	7	1.2554	3.8×10^{-3}	T_2 (85.2%), T_6 (5.4%), S_4 (2.3%)
	8	1.4225	0.49	S_2 (52.0%), T_3 (26.6%), T_6 (18.6%)

* Triplet states with contributions < 5% are not shown.

5. Photophysics

a) Solution state

Table S5.1. Photophysical characteristics of complexes **5** and **6** as well as reference complexes **8** and **9** in dilute solution at room temperature.

Complex	Solvent	λ_{abs} / nm (ε / 10^3 M^{-1} cm^{-1}) [a]	λ_{em} / nm [b]	Φ_{PL} [c]	τ / µs [d]	k_r / 10^5 s^{-1} [e]	k_{nr} / 10^5 s^{-1} [f]
5	**Toluene**	532 (20.2), 495sh (12.1), 421 (19.8), 406sh (18.4), 353 (28.7), 336sh (30.5), 311sh (46.7)	576, 611sh	0.11	0.34	3.3	26
	Chlorobenzene	532 (19.8), 495sh (12.6), 450 (10.0), 420 (21.0), 404sh (19.2), 354 (34.4), 336sh (33.1), 311sh (48.4)	576, 611sh	0.45	2.1	2.1	2.6
6	**Toluene**	577 (17.2), 536 (13.9), 510 (13.1), 475sh (15.2), 441sh (23.8), 422 (25.5), 347 (56.5), 329 (69.0), 314 (74.7)	627	0.23	0.40	5.7	1.9
	Chlorobenzene	-	-	-	-	-	-
8	**Toluene**	522 (15.0), 403 (16.8), 350 (23.1), 337 (22.6), 306 (33.2)	579sh, 617	0.16	1.2	1.3	7.1
	Chlorobenzene	525 (15.2), 450 (7.6), 401 (16.3), 373 (17.1), 351 (25.5), 336 (23.4), 306 (31.8)	578sh, 635	0.51	5.0	1.0	1.0
9	**Toluene**	575 (10.3), 536 (8.8), 509 (8.4), 475 (8.7), 443 (10.8), 415 (18.8), 368sh (22.3), 339 (30.4), 318sh (35.8), 309 (36.7)	628	0.43	1.0	4.3	5.6
	Chlorobenzene	571 (10.1), 538 (8.2), 511 (7.9), 473sh (7.5), 411 (16.8), 363sh (23.4), 337 (27.0), 311 (31.3)	633	0.57	1.7	3.3	2.5

[a] Absorption maxima and molar absorption coefficients; [b] Emission maxima; [c] Photoluminescence quantum yield recorded against rhodamine 6G (Φ_{PL}=0.91[2]) in air-equilibrated absolute ethanol solutions, [d] Photoluminescence lifetime at room temperature; [e] Observed radiative rate constant, $k_r = \Phi_{PL}/\tau$; [f] Observed non-radiative rate constant, $k_{nr} = (1-\Phi_{PL})/\tau$. Figures for complexes **8** and **9** were reproduced from previous works.[20,21]

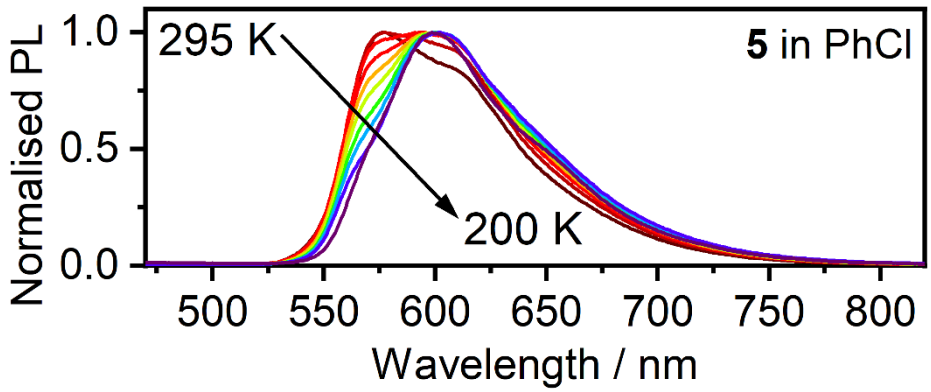

Figure S5.1. Steady-state photoluminescence spectra of **5** in a dilute (c = 10^{-5} M) solution in chlorobenzene (PhCl) recorded in the temperature range indicated.

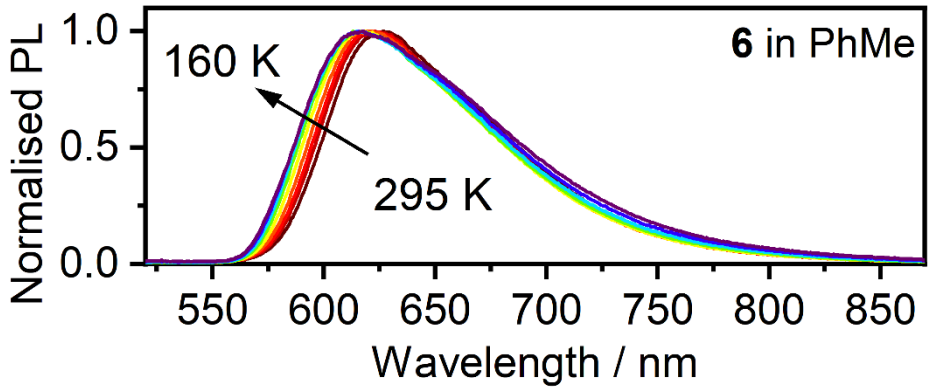

Figure S5.2. Steady-state photoluminescence spectra of **6** in a dilute (c = 10^{-5} M) solution in chlorobenzene (PhCl) recorded over the temperature range indicated.

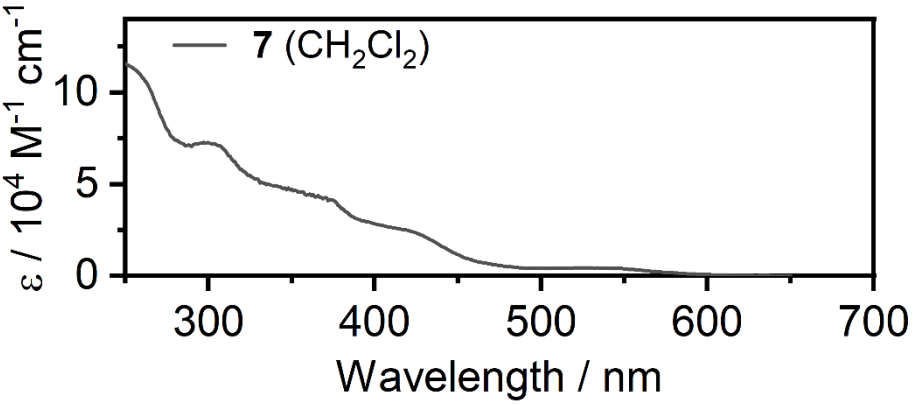

Figure S5.3. Absorption spectrum of Pt(IV) complex **7** in a dilute CH_2Cl_2 solution at 295 K.

b) Solid state

Table S5.2. Photophysical characteristics of complexes **5** and **6** as well as reference complexes **8** and **9** in polystyrene dispersions.

	5	**6**	**8**	**9**
λ_{em} / nm [a] (295 K)	575, 611sh	624, 667sh	579sh, 640	618
τ / µs [b] (295 K)	2.4	1.2	5.3	2.5
τ / µs [c] (80 K)	17.6	12.5	12.3	14.3
k_r^S / s [d]	4×10^7	3×10^7	9×10^7	1×10^7
ΔE_{ST} (fit) / eV [e]	0.094 ± 0.011	0.066 ± 0.002	0.159 ± 0.020	0.058 ± 0.003
S_1 / eV [f]	2.28	2.14	2.30	2.20
T_1 / eV [g] (80 K)	2.21	2.09	2.10	2.14
ΔE_{ST} (spec) / eV [h]	0.07	0.05	0.20	0.06

[a] Emission maxima; [b] Photoluminescence lifetime at room temperature; [c] Photoluminescence lifetime at 80 K; [d] Singlet radiative decay rate; [e] Singlet-triplet energy gap from the fitting; [f] Singlet energy recorded from fluorescence (TADF) spectrum onset at room temperature; [g] Triplet energy recorded from phosphorescence spectrum onset at 80 K; [h] Singlet-triplet energy splitting from fluorescence and phosphorescence spectra. Figures for complexes **8** and **9** were reproduced from previous works.[20,21]

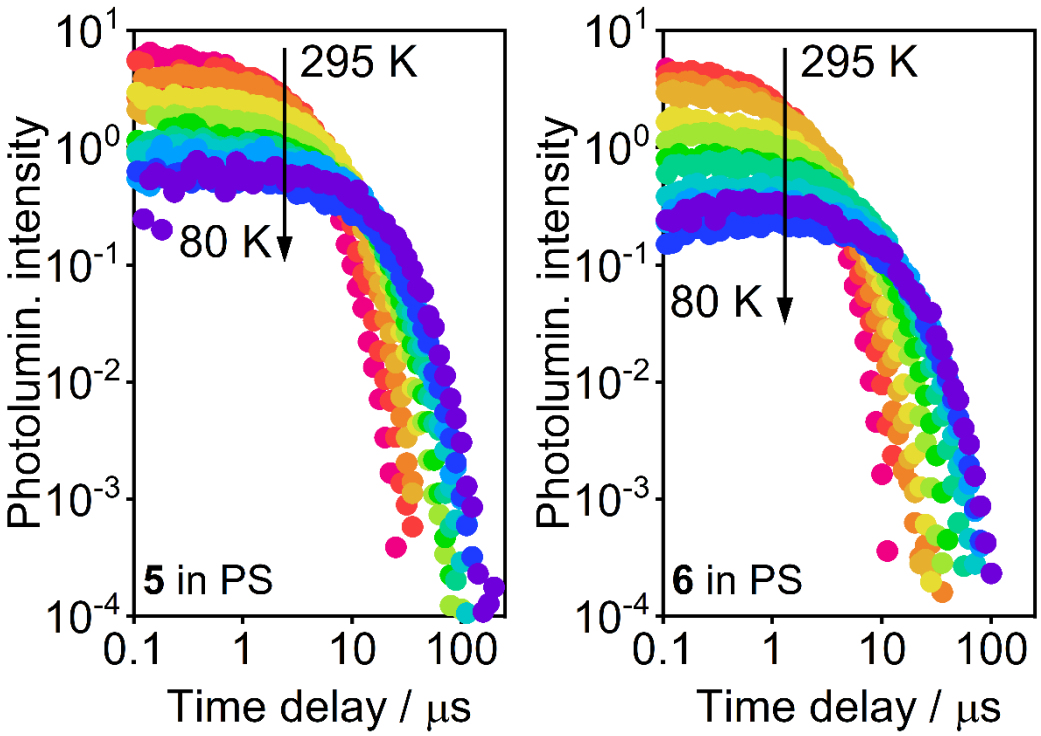

Figure S5.4. Photoluminescence decay of **5** and **6** recorded in polystyrene (PS) dispersion (c = 0.2% w/w) recorded in the temperature range indicated.

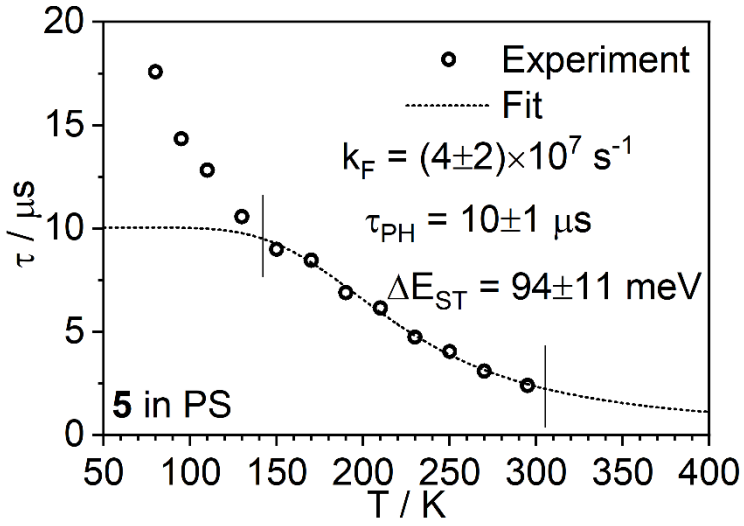

Figure S5.5. Changes in the monoexponential decay lifetime of **5** in polystyrene (PS) dispersion (c = 0.2% w/w) in function of temperature. Vertical lines indicate data range used for fitting.

6. OLEDs

Table S6.1. Characteristics of OLED devices 1-6 using **6** as the emitter.

	Dev 1	**Dev 2**	**Dev 3**	**Dev 4**	**Dev 5**	**Dev 6**
Emitter	**6**	**6**	**6**	**6**	**6**	**6**
V_{ON} / V [a]	8.7	8.7	7.6	8.3	7.4	8.3
L_{max} / mW cm^{-2} [b]	7600	4900	8700	8700	5400	3500
λ_{EL} / nm [c]	616	619	606	610	604	608
CE_{max} / cd A^{-1} [d]	9.3	6.6	15.8	13.2	17.8	13.5
EQE_{max} / % [e]	6.6	5.3	9.2	8.6	10.0	8.4
EQE_{mean} / % [f]	6.1	5.0	8.7	8.4	9.1	7.8
EQE_{median} / % [g]	6.1	5.0	8.8	8.4	9.0	7.8

[a] turn-on voltage at 1 cd m^{-2}; [b] maximum luminance; [c] electroluminescence spectrum maxima; [d] current efficiency; [e] maximum external quantum efficiency; [f] mean external quantum efficiency; [g] median external quantum efficiency.

Table S6.2. Characteristics of OLED device with **9** as the emitter (structure as in Dev 6).

	Dev 7
Emitter	**9**
L_{max} / mW cm^{-2}	1840
λ_{EL} / nm	612
EQE_{max} / %	2.29

See table above for explanation of the symbols used.

Table S6.3. OLED architecture for devices 1-6 presented in the main article.

Device	**Architecture**
Dev 1	ITO | AI4083 (30 nm) | TCTA:PO-T2T (80:20) co. **6** (3%) (~65 nm) | PO-T2T (50 nm) | LiF (0.8 nm) | Al (100 nm)
Dev 2	ITO | AI4083 (30 nm) | TCTA:PO-T2T (80:20) co. **6** (5%) (~65 nm) | PO-T2T (50 nm) | LiF (0.8 nm) | Al (100 nm)
Dev 3	ITO | AI4083 (30 nm) | PVKH (10) | mCP:PO-T2T (70:30) co. **6** (3%) (~30 nm) | PO-T2T (50 nm) | LiF (0.8 nm) | Al (100 nm)
Dev 4	ITO | AI4083 (30 nm) | PVKH (10) | mCP:PO-T2T (70:30) co. **6** (5%) (~30 nm) | PO-T2T (50 nm) | LiF (0.8 nm) | Al (100 nm)
Dev 5	ITO | AI4083 (30 nm) | PVKH (10) | mCP:PBD (60:40) co. **6** (3%) (~30 nm) | TmPyPB (50 nm) | LiF (0.8 nm) | Al (100 nm)
Dev 6	ITO | AI4083 (30 nm) | PVKH (10) | mCP:PBD (60:40) co. **6** (5%) (~30 nm) | TmPyPB (50 nm) | LiF (0.8 nm) | Al (100 nm)

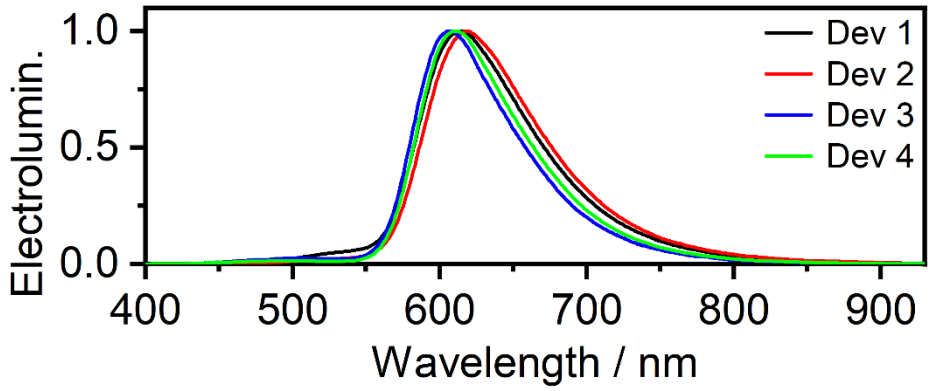

Figure S6.1. EL spectra of OLEDs 1-4.

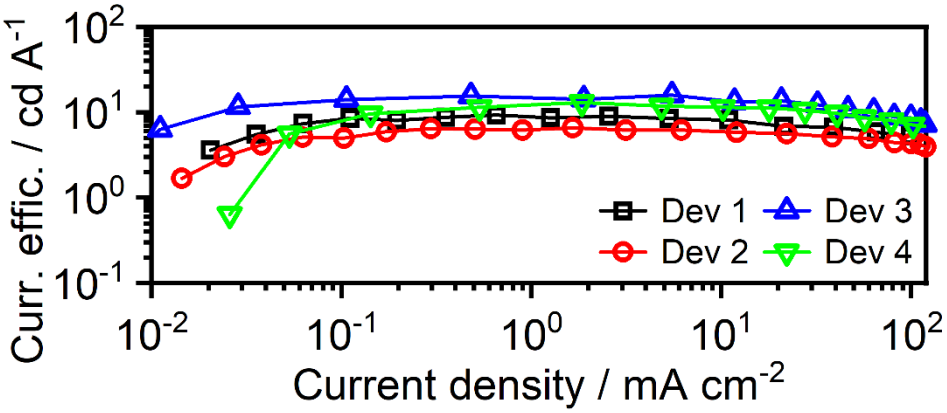

Figure S6.2. Current density-current efficiency characteristics of Devices 1-4.

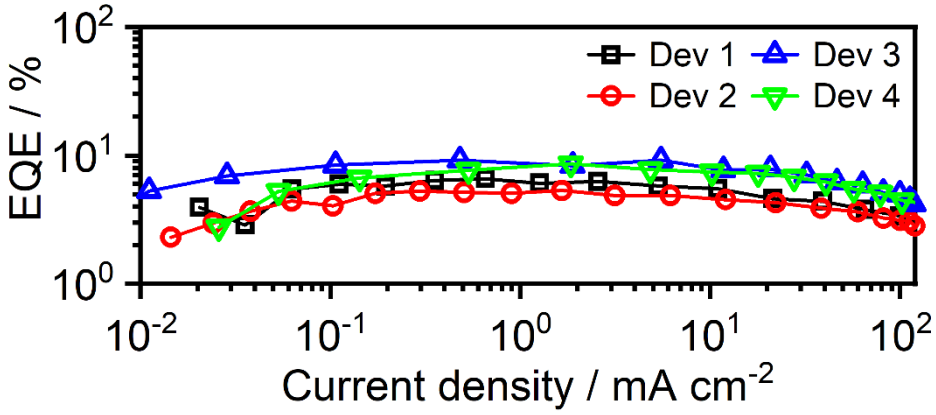

Figure S6.3. Current density-external quantum efficiency characteristics of Devices 1-4.

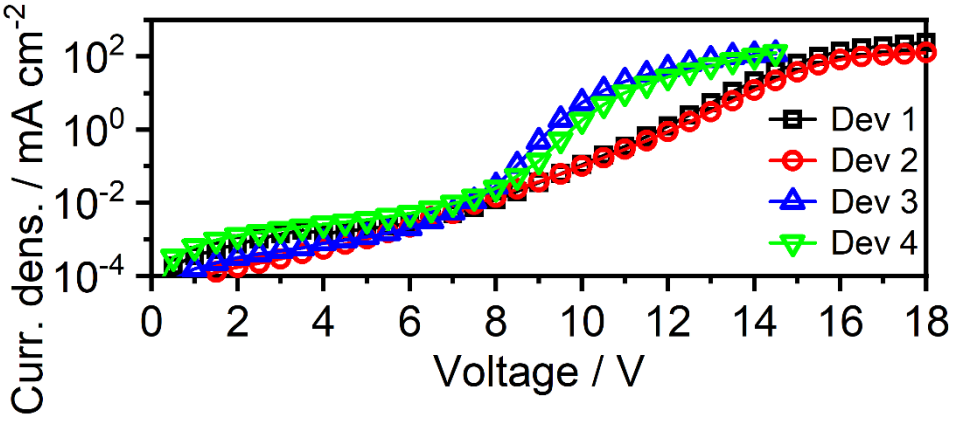

Figure S6.4. Voltage bias-current density characteristics of Devices 1-4.

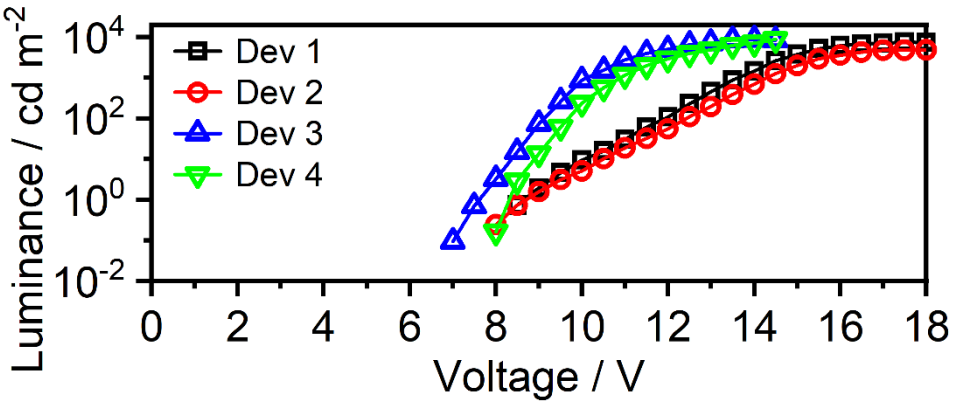

Figure S6.5. Voltage bias-luminance characteristics of Devices 1-4.

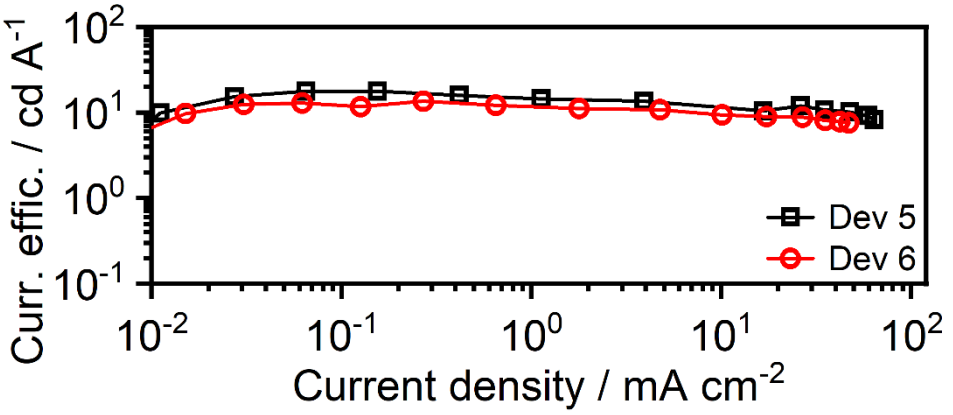

Figure S6.6. Current density-current efficiency characteristics of Devices 5 and 6.

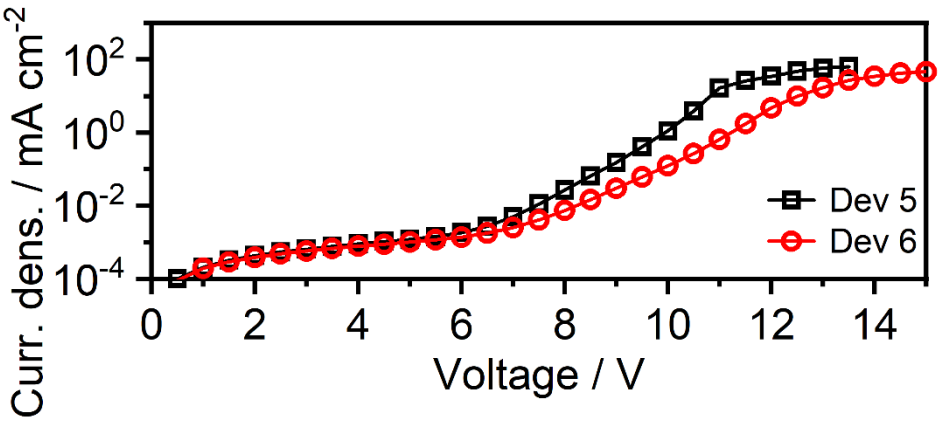

Figure S6.7. Voltage bias-current density characteristics of Devices 5 and 6.

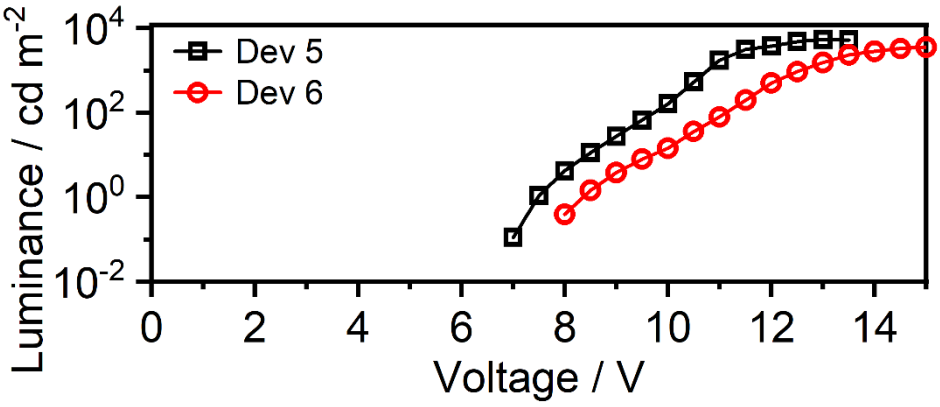

Figure S6.8. Voltage bias-luminance characteristics of Devices 5 and 6.

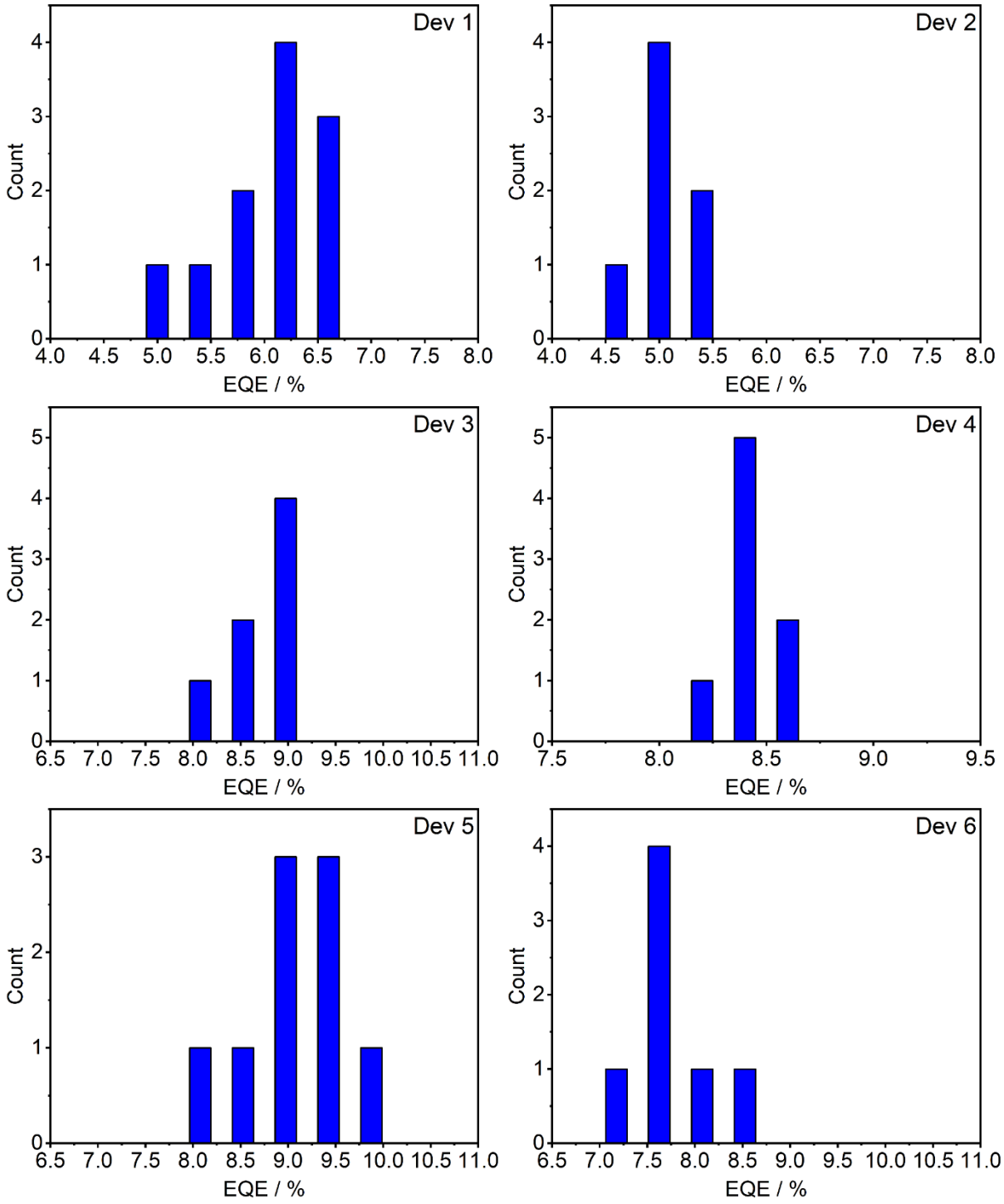

Figure S6.9. Distribution of external quantum efficiency values reported for OLEDs 1-6.

7. References

[1] P. Pander, P. Data, F. B. Dias, *J. Vis. Exp.* **2018**, DOI: 10.3791/56614.
[2] C. Würth, M. Grabolle, J. Pauli, M. Spieles, U. Resch-Genger, *Nat. Protoc.* **2013**, *8*, 1535.
[3] J. R. Kirchhoff, R. E. Gamache, M. W. Blaskie, A. A. Del Paggio, R. K. Lengel, D. R. McMillin, *Inorg. Chem.* **1983**, *22*, 2380.
[4] H. Yersin, A. F. Rausch, R. Czerwieniec, T. Hofbeck, T. Fischer, *Coord. Chem. Rev.* **2011**, *255*, 2622.
[5] D. de Sa Pereira, A. P. Monkman, P. Data, *J. Vis. Exp.* **2018**, DOI: 10.3791/56593.
[6] M. Roemelt, D. Maganas, S. DeBeer, F. Neese, *J. Chem. Phys.* **2013**, *138*, 204101.
[7] B. de Souza, G. Farias, F. Neese, R. Izsák, *J. Chem. Theory Comput.* **2019**, *15*, 1896.
[8] E. van Lenthe, E. J. Baerends, J. G. Snijders, *J. Chem. Phys.* **1993**, *99*, 4597.
[9] E. van Lenthe, E. J. Baerends, J. G. Snijders, *J. Chem. Phys.* **1994**, *101*, 9783.
[10] F. Neese, *WIREs Comput. Mol. Sci.* **2012**, *2*, 73.
[11] F. Neese, *WIREs Comput. Mol. Sci.* **2022**, *12*, DOI: 10.1002/wcms.1606.
[12] F. Weigend, R. Ahlrichs, *Phys. Chem. Chem. Phys.* **2005**, *7*, 3297.
[13] F. Weigend, *Phys. Chem. Chem. Phys.* **2006**, *8*, 1057.
[14] S. Grimme, S. Ehrlich, L. Goerigk, *J. Comput. Chem.* **2011**, *32*, 1456.
[15] S. Grimme, J. Antony, S. Ehrlich, H. Krieg, *J. Chem. Phys.* **2010**, *132*, 154104.
[16] D. A. Pantazis, X. Y. Chen, C. R. Landis, F. Neese, *J. Chem. Theory Comput.* **2008**, *4*, 908.
[17] A.-R. Allouche, *J. Comput. Chem.* **2011**, *32*, 174.
[18] O. V. Dolomanov, L. J. Bourhis, R. J. Gildea, J. A. K. Howard, H. Puschmann, *J. Appl. Crystallogr.* **2009**, *42*, 339.
[19] G. M. Sheldrick, *Acta Crystallogr. Sect. A Found. Crystallogr.* **2008**, *64*, 112.
[20] P. Pander, A. V. Zaytsev, A. Sil, J. A. G. Williams, V. N. Kozhevnikov, F. B. Dias, *J. Mater. Chem. C* **2022**, *10*, 4851.
[21] P. Pander, A. V. Zaytsev, A. Sil, J. A. G. Williams, P.-H. Lanoe, V. N. Kozhevnikov, F. B. Dias, *J. Mater. Chem. C* **2021**, *9*, 10276.